DEVELOPMENT OF POLY(LACTIC ACID)/LIGNIN COMPOSITE FILMS COATED WITH

BEESWAX FOR FOOD PACKAGING APPLICATIONS

By

MISS Arphaphorn ARJHAN

A Thesis Submitted in Partial Fulfillment of the Requirements

for Master of Engineering (CHEMICAL ENGINEERING)

Department of CHEMICAL ENGINEERING

Graduate School, Silpakorn University

Academic Year 2021

Copyright of Silpakorn University

การพัฒนาฟิล์มผสมระหว่างพอลิแลคติกแอซิดและลิกนินที่เคลือบด้วยขี้ผึ้งสำหรับการใช้บรรจุภัณฑ์อาหาร

โดย
นางสาวอาภาพร อาจหาญ

วิทยานิพนธ์นี้เป็นส่วนหนึ่งของการศึกษาตามหลักสูตรวิศวกรรมศาสตรมหาบัณฑิต
สาขาวิชาวิศวกรรมเคมี แผน ก แบบ ก 1 ระดับปริญญามหาบัณฑิต
ภาควิชาวิศวกรรมเคมี
บัณฑิตวิทยาลัย มหาวิทยาลัยศิลปากร
ปีการศึกษา 2564

DEVELOPMENT OF POLY(LACTIC ACID)/LIGNIN COMPOSITE FILMS

COATED WITH BEESWAX FOR FOOD PACKAGING APPLICATIONS

By

MISS Arphaphorn ARJHAN

A Thesis Submitted in Partial Fulfillment of the Requirements

for Master of Engineering (CHEMICAL ENGINEERING)

Department of CHEMICAL ENGINEERING

Graduate School, Silpakorn University

Academic Year 2021

| Title | Development of poly(lactic acid)/lignin composite films coated with beeswax for food packaging applications |
|---|---|
| By | Arphaphorn ARJHAN |
| Field of Study | (CHEMICAL ENGINEERING) |
| Advisor | Associate Professor Sirirat Wacharawichanant , D.Eng. |

Graduate School Silpakorn University in Partial Fulfillment of the Requirements for the Master of Engineering

----- Dean of graduate school

(Associate Professor Jurairat Nunthanid, Ph.D.)

Approved by

----- Chair person

(Associate Professor Prakorn Ramakul , D.Eng.)

----- Advisor

(Associate Professor Sirirat Wacharawichanant , D.Eng.)

----- Co advisor

(Associate Professor Pakorn Opaprakasit , Ph.D.)

----- Committee

( Sunthon Piticharoenphun , Ph.D.)

----- External Examiner

(Professor Anongnat Somwangthanaroj , Ph.D.)

620920075 : Major (CHEMICAL ENGINEERING)

Keyword : Poly(lactic acid), Casting films, Packaging, Lignin, Beeswax, Coating

MISS ARPHAPHORN ARJHAN : DEVELOPMENT OF POLY(LACTIC ACID)/LIGNIN COMPOSITE FILMS COATED WITH BEESWAX FOR FOOD PACKAGING APPLICATIONS THESIS ADVISOR : ASSOCIATE PROFESSOR SIRIRAT WACHARAWICHANANT, D.Eng.

In this work, PLA/lignin composite films have been developed for packaging applications. The composite films were prepared by a solution casting method. The lignin was prepared from black liquor from the paper industry, by extracting with acetic acids at 50°C. Scanning electron microscopy (SEM) was used to study the size and shape of the lignin particles. The lignin contents in PLA matrix were 0.5, 1, 3 and 5 phr. The SEM results showed that as the lignin content increased, the surface roughness and voids increased except at 1 phr and 5 phr. Fourier-transform infrared (FTIR) spectroscopy was used to study the interactions between PLA and lignin. The results of the PLA/lignin composite film showed a reduction crystalline with the change of the diffraction peak around $2\theta = 19°$ by X-ray diffraction (XRD). The lignin reduced the tensile strength of PLA/lignin films, whereas the composite film at 1 phr of lignin was more elongation than neat PLA. Thermal stability of PLA/lignin composite films increased with the addition of lignin. UV-Vis analysis indicated reduced light transmission with increasing lignin contents in UV region. The scavenging activity also increased with the amount of lignins by DPPH method. The lignin increases the impermeable physical barriers in the PLA so reducing the effect of water vapor transmission rate (WVTR). The addition of lignin to PLA did not significantly change the contact angle of PLA. Then select the appropriate amount of lignin for beeswax coating. The beeswax dipping coating maintains the film good mechanical and antioxidant properties. The film obtained after the coating increased roughness by SEM and increased water contact angle by WCA measurement as the beeswax concentration increases.

# ACKNOWLEDGEMENTS

# TABLE OF CONTENTS

# LIST OF TABLES

# LIST OF FIGURES

# CHAPTER 1

# INTRODUCTION

Nowadays, biodegradable packaging has advantages over synthetic plastics such as biodegradability or compostability and renewable raw materials. Both of these are commercial interest in the packaging industry for food to meet the needs of the market and consumers. Compostable and recyclable packaging materials contain bio-polymers and paper products [1]. These materials can be degraded into simpler substances by using water and carbon dioxide or making it into small molecules when exposed to an open environment with optimal temperature, humidity, the amount of oxygen and microorganisms that will be biodegradable [2].

Food packaging takes into consideration of the protection and preservation of food quality during its processing, storage, handling and marketing. The food packaging industry has developed ways to preserve food quality, extend shelf life, food safety and reduce the food-borne diseases by reducing the effects of oxidation and action of microorganisms in food. Therefore, active food packaging has become a new technology that meets the needs of consumers and the market. These are designed to extend the shelf life of food. Good packaging must be able to protect food from environmental effects such as moisture, gas ($O_2$, $CO_2$), heat, light, odor, pressure, dirt, insects, and microorganisms. It also provides antimicrobial and antioxidant properties and can reduce the any mechanical damage [3].

Poly(lactic acid) (PLA) is a type of biodegradable thermoplastic material made from lactic acid. When exposed to moisture and microorganisms, PLA is naturally metabolized [4]. In addition to its biodegradable properties, PLA has mechanical properties that are comparable to poly(ethylene terephthalate) (PET) and better than polystyrene (PS) due to its hardness and stiffness. However, the major drawback is its

brittleness due to low crystallinity. Many methods are used to modify PLA, such as copolymerization and blends. PLA is a bio-based polymer with high mechanical strength, stable thermal behavior and biocompatibility properties. Typically, PLA-based packaging films have excellent food barrier properties compared to conventional petroleum-based films [5]. Although PLA is biodegradable with many interesting properties. The limitations of PLA are high brittleness, low softening temperature and weak water vapor properties and gas barrier properties, lower moisture sensitivity.

Lignin is the second most important component of woods. Lignin is available in a wide range of quantities as a by-product of the production of cellulose pulp in the production of paper [6]. Lignin is made up of three phenols linked by ether bonds and different functional groups can be found in different proportions of lignin. There are also functional groups that ultraviolet (UV) radiation absorbing functional groups, such as phenolic unit, ketone and chromophores [7]. These functional groups provide lignin with excellent UV blocking ability as well as antioxidant and free radical scavenging properties. More recently, lignin has been used as a thermostat, antioxidant, reinforcement and compatible agent for the preparation of polymer composites and blends. Lignin is also considered a sustainable drug and alternative to polyacrylonitrile as a carbon precursor.

Beeswax is a complex product that is released in liquid form by special wax glands in the abdomen of young worker bees when exposed to air, it freezes in scales [8]. Biological wax can provide low surface energy. The collaboration of low surface energy and micro/nano structures results in high water contact angles and small sliding angles [9]. Beeswax is more resistant to moisture transport than most other fats and more effective than other natural ones [10]. Beeswax to improve the vapor barrier properties of PLA and biodegradable.

The main function of packaging for food products is to prevent deterioration of quality of the foods. Therefore, interests in developing packaging that can help maintaining the highest quality food products for as long as possible by reducing or limiting the factors that cause the deterioration of the quality of the food to be maintained. The packaging acts as a barrier between the product and the external environment. PLA has high mechanical strength, stable thermal behavior, but lacks the property to prevent food deterioration. Lignin was added to aid in UV protection and to prevent oxidation. Finally, beeswax is applied to coat on the film to improve barrier properties. This work is intended to develop food packaging using PLA with optimum packaging properties. The addition of lignin provided UV protection and antioxidant protection. In addition, beeswax is introduced to coat on the film surfaces to improve the barrier properties, which can help lowering both water vapor permeation and oxygen permeability.
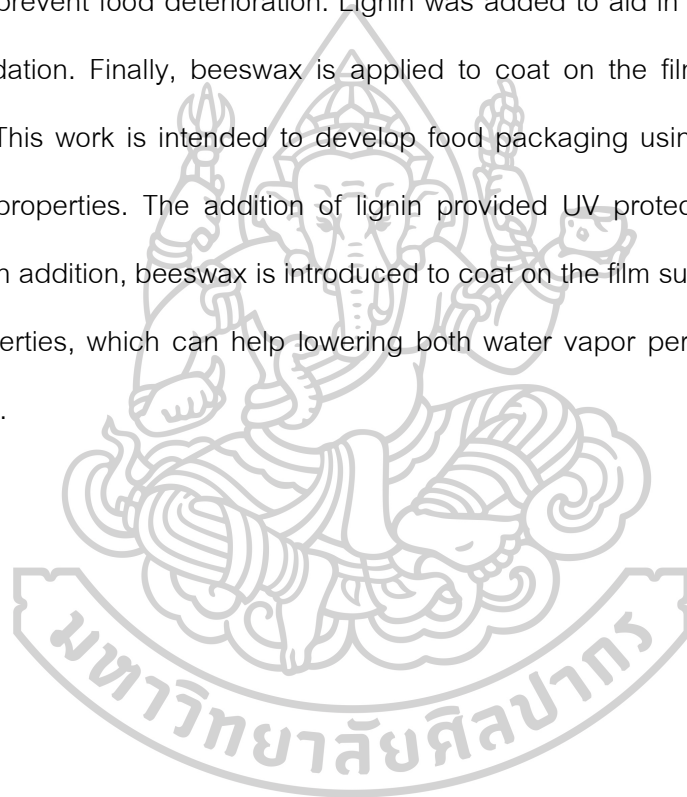
# CHAPTER 2

# THEORY

## 2.1 Poly(lactic acid) (PLA)

PLA is compostable, thermoplastic, and biocompatible polymer, which is made from renewable resources, such as corn, sugar beets and potato starch. PLA is commonly used as packaging materials. PLA degrades through the hydrolysis of backbone ester groups as shown in Figure 1. The degradation rate depends on the PLA crystallinity, molecular weight, molecular weight distribution, morphology, water diffusion rate into the polymer, and stereoisomeric content [11].
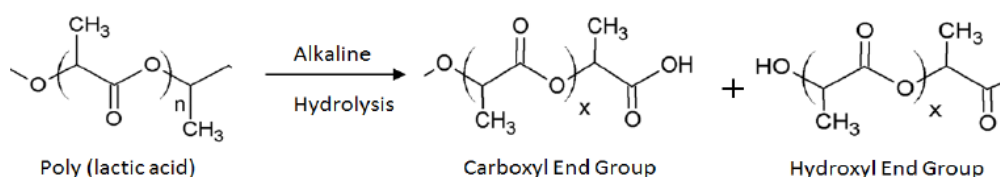


Figure  1 The hydrolysis of ester groups in PLA structure [12].

Lactide is a chiral molecule which is different arrangements of atoms around carbon have two forms L-lactide and D-lactide. There are several methods for synthesis of PLA, as illustrated in Figure 2. The most popular method is the ring-opening polymerization of lactide. The polymerization of lactide leads to the formation of semicrystalline PLA. PLA has three different structures: poly(L-lactide) (PLLA), poly(D-lactide) (PDLA), and poly(D,L-lactide). In packaging applications, poly(D,L-lactide) with 90% L-lactide has been widely used [11]. The D-lactide concentration with increased produces more crystalline structure for PLA polymers and PLA films with better thermal, mechanical, and barrier properties when PLA with a high D-lactide concentration is not common today due to its high cost.
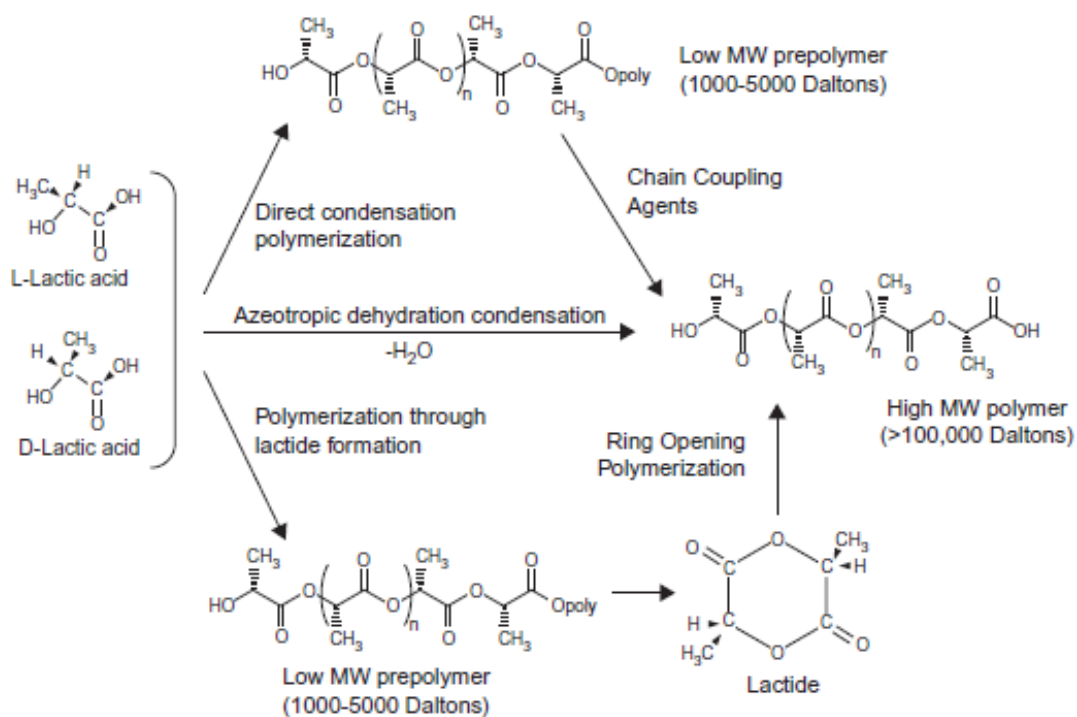
Figure  2 Synthesis of polylactic acid (PLA) from L- and D-lactic acids [11].

PLA has high transparency suitable for industrial applications, such as films, fibers, and bottles. Lactide is commonly discovered in plants and animals, as a by-product or intermediate product of metabolism, so PLA is nontoxic. PLA is biologically degradable by common microorganisms [13]. Currently, PLA used in industrial packaging and biomedical applications, because the processing possibilities of this transparent material are very wide, ranging from injection molding to blow molding and thermoforming [14]. Since PLA is brittle, blending with other polymers is needed to improve properties but still biodegradable polymers.

## 2.2 Lignin

Lignin is a biological substance that can be found in common wood, one of the most important raw materials in the industries, as shown in Figure 3. It presents structure of cell wall including lignin, cellulose and hemicellulose. Therefore, in the pulp production process, wood is required through the pulp boiling process to remove lignin. Since, lignin will cause paper to yellow when exposed to light. Eliminated lignin will be contaminate with water so called Black liquor. Black liquor is waste obtained from the pulp industries. Wood consists of cells and the cell walls consist mainly of three organic components including cellulose (40–60 wt%), hemicelluloses (25–35 wt%) and lignin (15–30 wt%) [15].
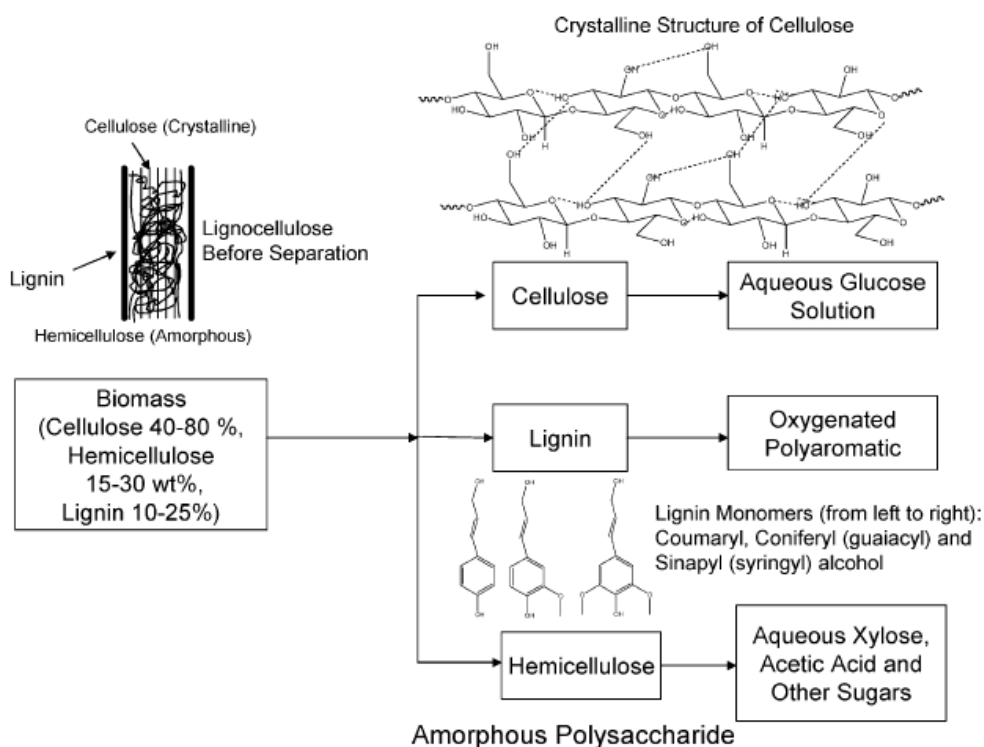


**Figure  3** Schematic structures of cell walls [16].

Lignin structure is highly asymmetrical, amorphous and contain the highly complex chemical nature of three different phenyl propane monomers refer to Figure 4. For the above reason, lignin does not have a regular structure like cellulose, but is a physically and chemically heterogeneous material, although the exact chemical structure is unknown [17].
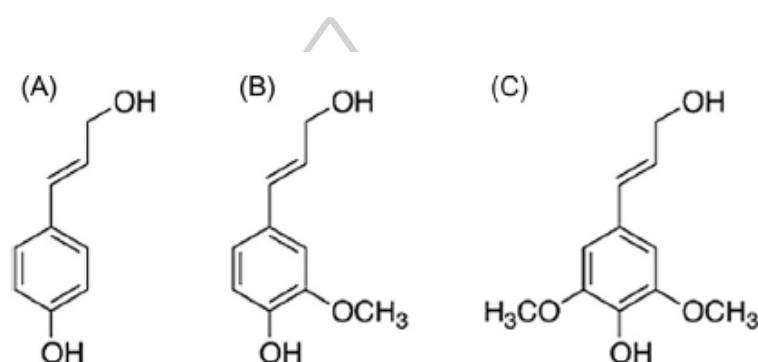


**Figure 4** Three different phenyl propane monomers (A) p-coumaryl alcohol; (B) coniferyl alcohol; (C) sinapyl alcohol [18].

Lignin is a polar hydrophilic biopolymer with biodegradability, antioxidant and reinforcing capability. These properties make lignin a potential candidate to improve the properties of thermoplastic polymers. Lignin could be blend with polymers to improve their properties such as antioxidant, thermal stability, mechanical performance (impact, stiffness, strength and elongation properties), UV stability, and biodegradability [15]. Lignin has the appropriate chemical properties for use in composites and coatings because lignin is hydrophobic in nature, has small particle sizes, and has ability to form stable mixtures.

## 2.3 Beeswax

Beeswax is produced mainly by specialized beeswax manufacturers. Beeswax is a natural wax composed of a mixture of esters (67 wt%) hydrocarbons (14 wt%), fatty acids (12 wt%), alcohol (1 wt%) and other compounds like aromatic substances and pigments (6 wt%) [19]. Production of good beeswax depend on method production which wax extraction have two method: melting and chemical extraction. Melting is the most frequently used procedure and chemical extraction by solvents is feasible only in a laboratory, where small scale wax production is needed. Good wax solvents are gasoline and xylene which disadvantage of this method is that all organic wax contaminants and constituents of the pupae, propolis and pollen are dissolved [20]. The color of newly made beeswax is clear white but after manipulating the honeybees it changes to yellow, dark yellow and brownish originated from propolis and pollen pigments [21].

Beeswax is added to paints, polish, cosmetics and is used for coating food and tablets [22]. Beeswax is a substance that helps build the structure of honeycomb by bees secrete beeswax for build honeycomb. Beeswax has hydrophobic protective properties which is in fact present within cosmetics and body products. Beeswax is used in the food industry such as a film to wrap cheese for maturing or as a food additive to give shine to the products [8].

## 2.4 Solution Casting and Coating Method

The first process, polymer and all ingredients were dissolved in common solvent and stirred until homogeneous solution, followed by this solution cast on glass plate or petri dish, called a solution casting method. After evaporation, the film was peeled off from glass plate. All above the process is presented in Figure 5.
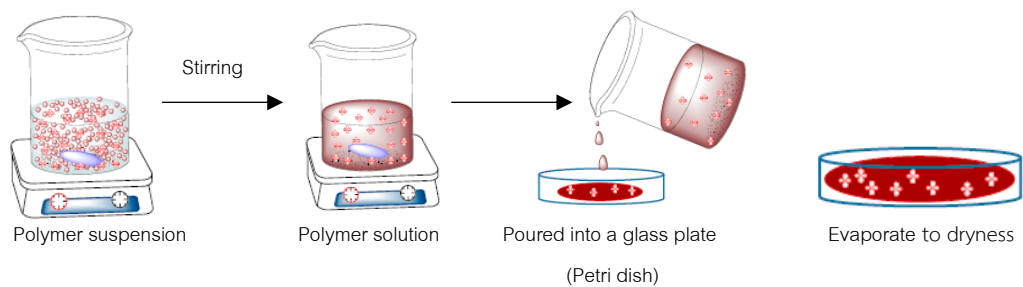
**Figure  5** Solution casting method [23].

The second process, this technique used for fabricating thin composite films by solution coating method as depositing a thin selective layer on top of substrate or support according to Figure 6.
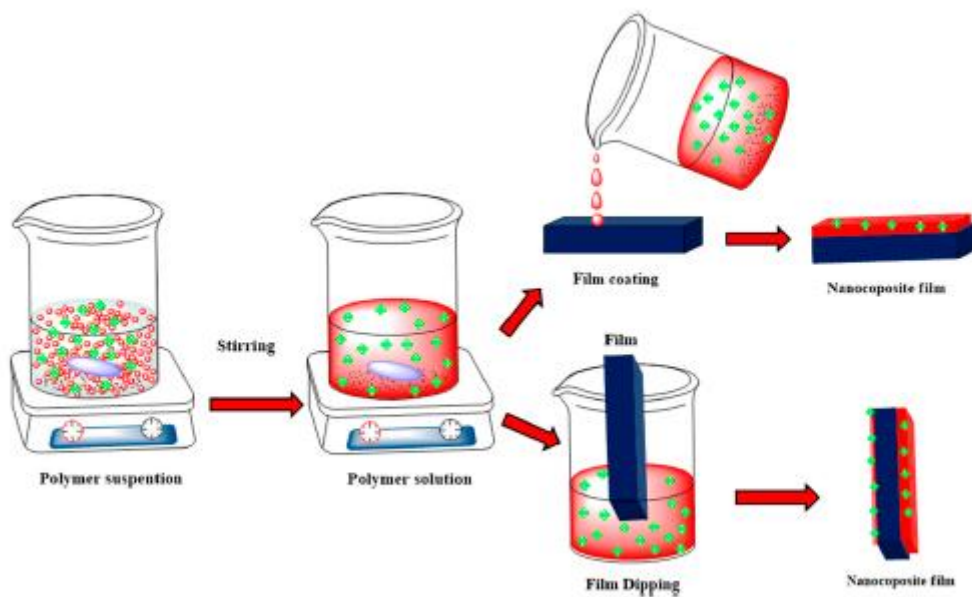


**Figure  6** Solution coating method [23].

## 2.5 Scanning Electron Microscopy (SEM)

SEM is electron microscope that produces images of a sample by scanning it with a beam of electrons [24]. The electron beam column consists of an electron gun, a condenser lens and an objective lens, as detailed in Figure 7 [25]. The electron gun emits a beam of electron when electrons hit the surface of a sample containing atoms, it emits a signal that can be process and give information including estimating surface roughness, characterizing the corrosion pits (their dimension and shape), locating the corrosion and determining the morphology of corrosion products (such as oxides) [26]. These interactions and effects between electrons in the beam interact with the atoms are detected and transformed into an image. Distinctive point of SEM is high depth of field and high spatial resolution because SEM used the smallest wavelength of the illuminating sources therefore the best resolution of the microscope [27].
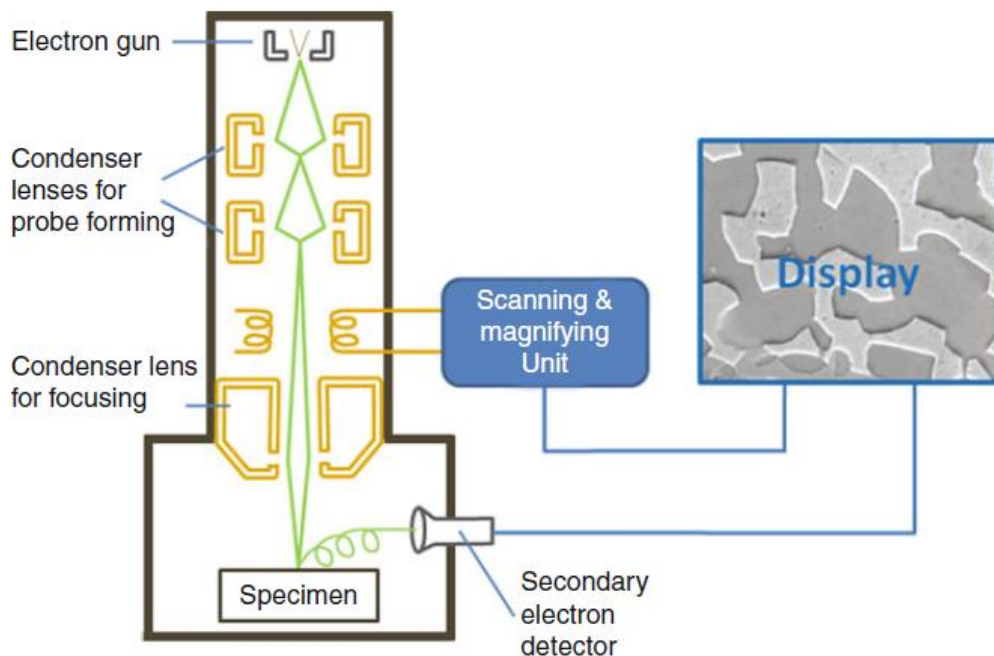


**Figure  7** Schematic of Scanning Electron Microscopy (SEM) [28].

2.6 Universal Tensile Testing

Universal testing machine (UTM) is a mechanical property tester, commonly called a tensile device, as reported in Figure 8. This instrument is capable of tensile test, tear resistance test, hardness test, compression test, bending test and other testing of various specimens including plastics, composites, rubber, fibers, etc., depending on equipment support. The principle of instrument working is collection of the relationship between resistance measurement in material deformation by using a force measuring device or load cell and measuring distance change of a specimen by a distance-measuring device, such as extension of crosshead and extensometer. The size or dimensions of the specimen are calculated that will be relationship graph between stress and strain resulting in various mechanical properties of the specimen such as modulus, strength and elongation. The test is referred to international standards, such as ASTM and ISO, which generally refer to requirements such as specimen size, number of specimens, testing speed, temperature, relative humidity, testing method, test results and other limitations or recommendations. This is for the benefit of comparing the test results [29].
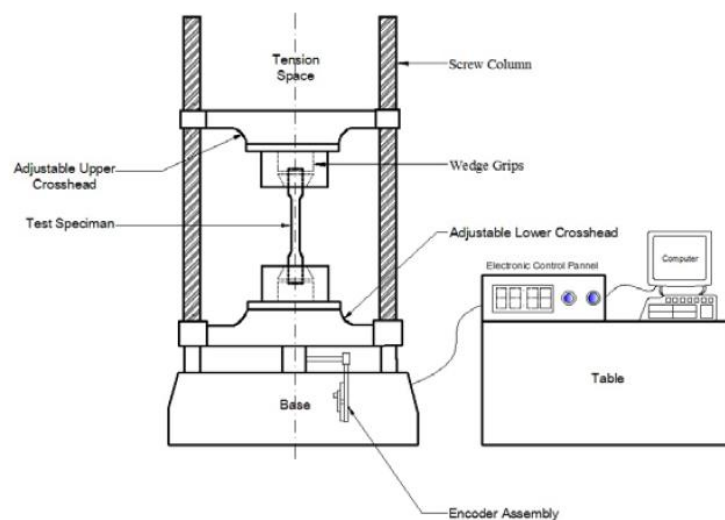


**Figure  8** Schematic diagram of Universal Tensile Testing (UTM) [30].

**2.7 Differential Scanning Calorimetry (DSC)**

Differential scanning calorimetry (DSC) is a popular technique used in the analysis for thermal property of materials. Differential scanning calorimeter measures the difference between heat flow to samples or exits a sample compared with a reference pan, measured as a function of temperature or time. DSC machines usually heat transfer, which is the transfer of energy (heat) per unit time, expressed in mJ/s or mW (y-axis) with time or temperature (x-axis) on the DSC heating curve. In case the sample absorbs energy (heat), the enthalpy transition is called "endothermic". In case the sample emits energy (heat), the enthalpy transition is called "exothermic". DSC heating curve shows the temperature and heat of the change (temperature and heat transition) temperature transitions, such as onset temperature ($T_o$), peak temperature ($T_p$) and end temperature ($T_e$), which are the initial temperature, the highest temperature and the last temperature of the changes. The area under the graph can be used to compute the enthalpy of transition ($\Delta$H, J/g) or the amount of heat to transition the energy (heat) required or released during transition which can also indicate the ordering of the sample. The amount of heat required to increase the temperature by the same increment ($\Delta$T) of a sample cell ($q_s$) is higher than that required for the reference cell ($q_r$) by the excess heat absorbed by the molecules in the sample ($\Delta$q), as illustrated in Figure 9. The resulting DSC scans with the reference subtracted from the sample show how this excess heat changes as a function of temperature [31].
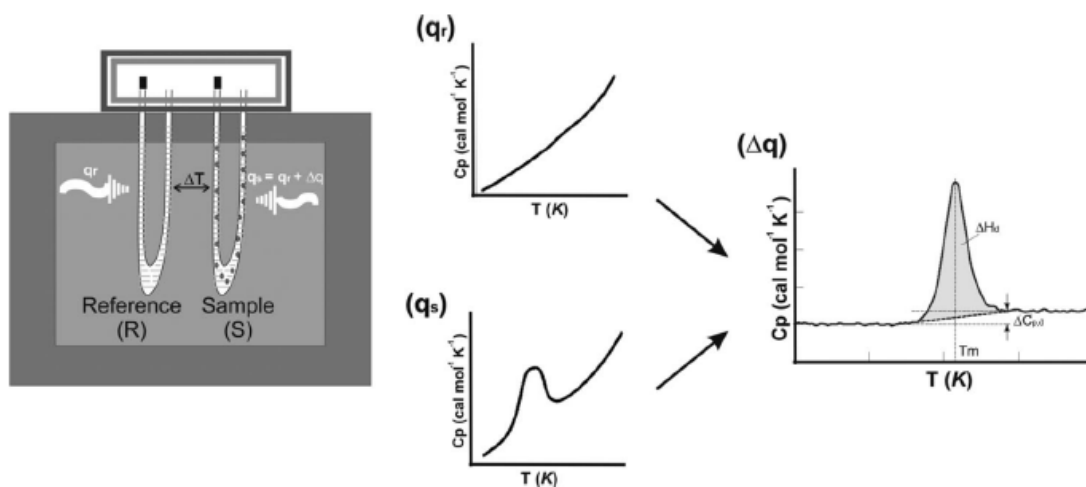
Figure 9 The concept of Differential Scanning Calorimetry (DSC) [31].

## 2.8 Thermogravimetric Analysis (TGA)

TGA is a technique used to analyze thermal stability of materials. In particular, when heated, the weight changes of materials in each temperature range are measured with a highly sensitive balance. This technique is suitable for the analysis of material dynamics involved in gas absorption or water evaporation, crystallization due to phase change, cracking of material (decomposition). In addition to this technique, study of oxidation and reduction reactions and stoichiometry. In sample analysis, the sample is placed on a small plate which is connected to a fine balance, that is highly sensitive where all are in the furnace that can control the temperature and atmosphere. The atmosphere inside can be inert gases, such as nitrogen or active gases, such as air or oxygen, with varying sample weights to occur at specific temperatures of each substance. The lost weight is caused by evaporation, degradation or reaction. The test results will be displayed in a graph with the y-axis shows the weight change (weight% or mg) and the x-axis shows the temperature or time, as reflected in Figure 10. The analysis of results requires a known chemical reaction and the decomposition

temperature of the sample roughly or contains information about the decomposition temperature of various reference samples compare the results [32].
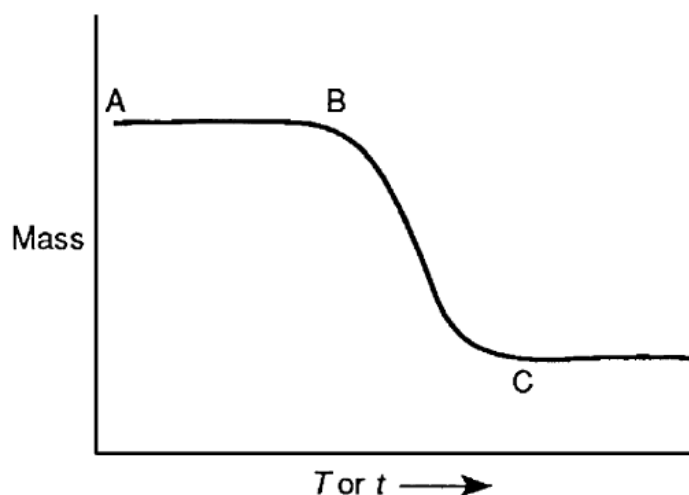


**Figure 10** TGA can be illustrated by reference to the single-stage process [32].

## 2.9 Fourier Transform Infrared (FTIR) Spectroscopy

Fourier Transform Infrared Spectrometer (FT-IR spectrometer) is an instrument used to analyze the structure of substances by measuring the absorption of radiation in the infrared range, which in the wave number of approximately 12800 - 10 cm$^{-1}$ also can be analyze samples of both solids, liquids and gases. Infrared radiation is electromagnetic radiation that is invisible to the naked eye, but produces heat that can be touched. Infrared radiation is between visible radiation and microwave radiation, which is divided into 3 regions: near infrared (12800-4000 cm$^{-1}$), mid infrared (4000-200 cm$^{-1}$) and far infrared (200-10 cm$^{-1}$). The range of infrared radiation useful in chemical analysis is the mid IR range when a molecule absorbs infrared radiation, it causes the bonds in the molecules to vibrate and spin that effect of causing molecular changes. From molecules to absorb infrared radiation, the frequency of infrared radiation must be equal to the oscillation frequency of the molecule substance. Each organic material has a specific and different frequency of oscillation, this technique is used in the analysis of

organic structures and types. The results obtained by this technique analysis show the relationship between wave number and transmittance, that called Infrared spectrum as illustrated in Figure 11 [33].
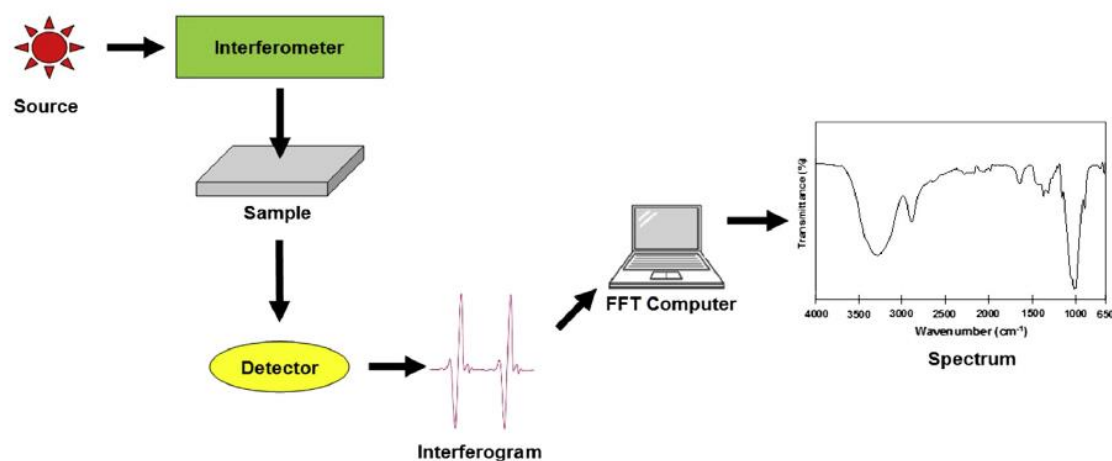


**Figure  11** Schematic illustrates the main component of a simple FTIR spectrophotometer [33].

## 2.10 X-Ray Diffraction (XRD)

X-ray diffraction analysis (XRD) is a technique that uses X-rays to analyze and identify compounds and crystal structure of compounds present in the sample for both qualitative and quantitative. X-ray diffraction analysis technique is based on the principle of firing incident X-ray radiation on the sample that cause diffraction and different angle reflection with a signal probe (detector) as a receiver, as shown in Figure 12. Composition and structure of a substance have X-ray diffraction degrees at different angles depend on the composition, shape and nature of the crystal that the result can indicate the type of compound present in the sample and can be used to study in detail the crystal structure of the sample. In addition, it can also be studied and analyzed as crystallinity, crystal size, crystal integrity and compound stress in the sample when

analyzing with accessories such as cooling-hot equipment can study the changes in the crystal structure in the test conditions change [34].
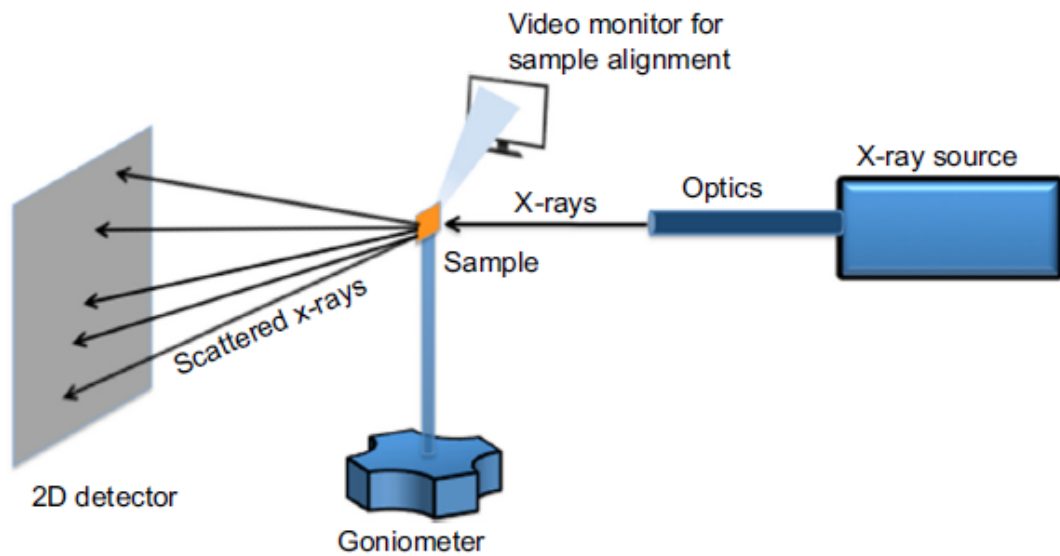


**Figure 12** Schematic representation of XRD machine [34].

This technique is based on constructive interference of monochromatic X-rays with a crystalline sample, as follows:

$$\lambda = 2d_{hkl} \sin(\theta_B) \tag{1}$$

This equation is Bragg's law and it relates the wavelength of the electromagnetic radiation ($\lambda$) with the diffraction angle ($\theta_B$) and the distance between two adjacent atomic planes ($d_{hkl}$) with indexes ($hkl$), according to the scheme presented in Figure 13 [29].
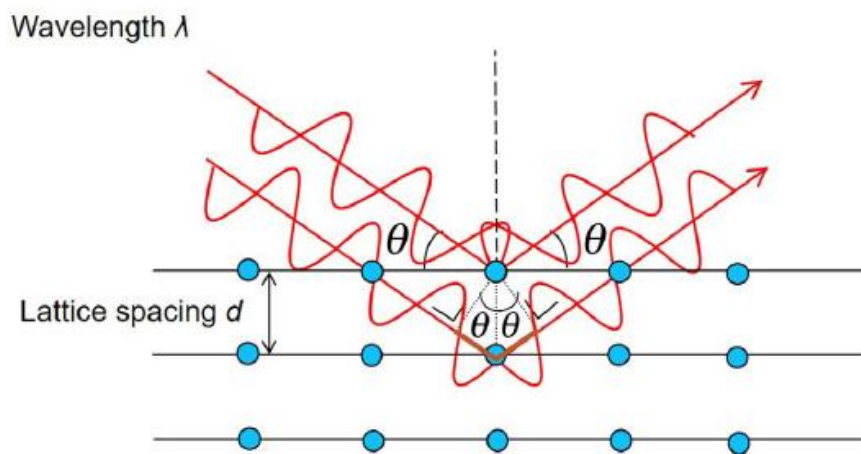
Figure 13 Scheme of X-ray diffraction (XRD) beam working principle [29].

## 2.11 Ultraviolet-Visible Spectroscopy (UV-Vis)

UV-Vis spectrophotometer is an instrument used in the analysis of substances based on the radiation absorption principle of substances in the ultraviolet (UV) and visible (Vis) range of wavelength approximately 190-1000 nm is mostly organic, inorganic and complex compounds both colored and colorless. Each substance absorbs radiation at a different wavelength and the amount of absorption depends on substance intensity. The absorption of various substances is directly proportional to the concentration of the substance that it can be analyzed in terms of both quality and quantity. This is a technique that provides better condition and widely used. The results obtained from this technique analysis show the relationship between the absorbance and wavelength, which is called the spectrum. A main component of a UV-Vis spectrophotometer is a light source. A radiation source is the part that emits radiation at the desired wavelength continuously as well as having enough light intensity. There are many types of radiation source lamps according to the radiated wavelength, such as the UV range, the H2 and D2 lamp are used for the wavelengths in the 160-380 nm and the Visible range uses Tungsten/halogen lamps that provide wavelength in the 240-2,500

nm. There are two light sources; one for ultraviolet light and one for visible light according to Figure 14. A mirror is used to select the proper light source. The diffraction grating is the monochromator that selects specific wavelengths of light. The two detectors are coupled so that reference absorptions can be subtracted from sample absorptions [35].
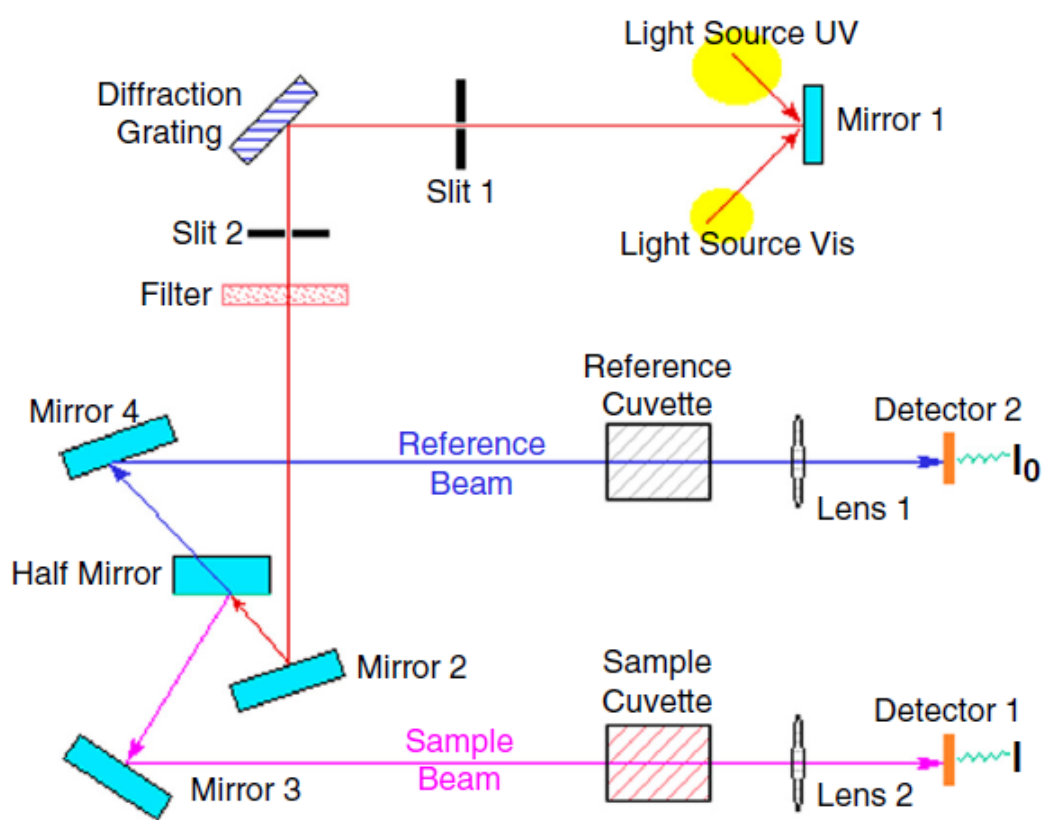


Figure 14 Diagram of Ultraviolet-Visible spectrophotometer [35].

## 2.12 Water Vapor Transmission Rate (WVTR)

Water vapor transmission rate (WVTR) refers to the speed of water vapor penetration through a material in a unit of grams/square meter/day. The water vapor permeability was measured in the equilibrium state at 38°C and at 90% relative humidity, the steam permeability of food-containing plastics that used for dry food packaging design as it is important for the shelf life of food. This machine will generate moisture or steam through a moisture generator by using nitrogen gas leads to moisture or steam enters the machine on top of the film where the humidity above is high humidity and below it carries nitrogen gas that pure nitrogen gas does not pass moisture. This machine continues testing in this state will find that the moisture above will gradually seep through the film wall by work must also depend on time. Therefore, the measurement equation has to time and area as a factor setting the values that WVTR is required to determine the permeability of water vapor [36].

## 2.13 Water Contact Angles (WCA)

The contact angle is used to measure the wettability of surfaces of materials. The wetting of a liquid drop above the material surfaces. How the droplet spread out and the boundary surface deposited on the material is measured. The wetting is determined by measuring the contact angle, which the liquid forms in contact with the material. The wetting trend to be larger, the smaller of the contact angle or the surface tension which a wetting liquid is a contact angle with the material is smaller than 90° whereas a non-wetting liquid creates a contact angle with the material is between 90° and 180°, as show in Figure 15. The traditional definition of a contact angle is the angle a liquid creates with the solid or liquid when it is deposited on it [37].
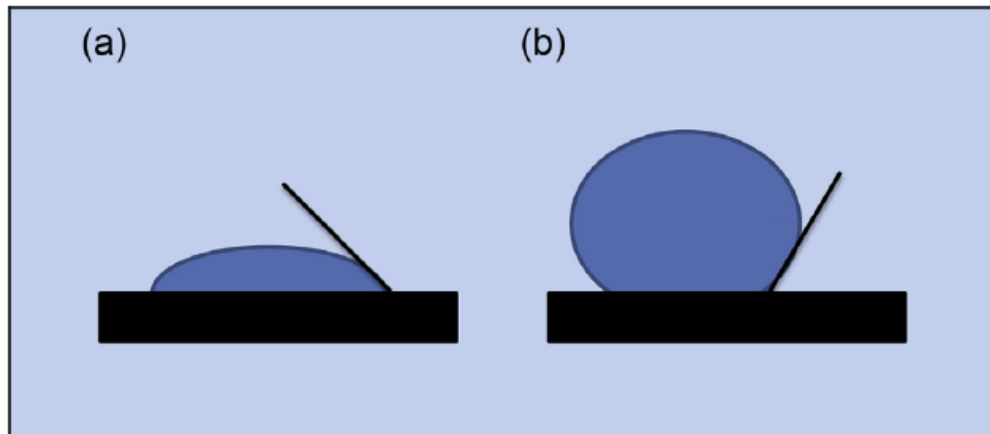
**Figure 15** Water contact angles on surface of materials; (a)<90° is wetting (b)≥90° is non-wetting [38].

## 2.14 Antioxidant

An important cause of food quality deterioration is lipid oxidation. Lipids are receptive to oxidation processes in the presence of catalysts such as heat, light, enzymes, metals, metalloproteins and microorganisms, which cause distorted flavors in food and loss of essential amino acids [39]. Therefore, the idea was to bring antioxidants together with food such as polyphenol compounds, vitamins C and E and carotenoids to support mechanisms in preventing oxidation [40]. Many oxidation tests use lipid oxidation stimulation using high temperature and high oxygen content which carries the risk of deterioration at the time of testing. The DPPH free radical method was chosen which eliminates the risk of degradation the thermal condition of the molecule [41]. DPPH is stable free radical and appears purple. DPPH assay is the principle that when DPPH solution is mixed with a substance capable of donating hydrogen atoms, it produces a reducing form with a purple loss [42]. DPPH accepts a hydrogen atom (H) from a scavenger molecule i.e. antioxidant, resulting in change a purple color to yellow. The discoloration is investigated by spectrophotometer and used to determine of parameter for antioxidant properties [43].

CHAPTER 3

LITERATURE REVIEWS

3.1 Lignin Precipitation

The structural difference of lignin is based on its separation process, which has been developed over many years in the separation of wood to extract lignin [44]. Typically, lignin is approximately 10-100 µm. The large amounts of lignin can be effect to mechanical properties. Therefore, it be used in appropriate amounts to polymer development [45]. Nowadays, organic acids are used to purify lignin, where organic acids are low-cost and non-polluting for precipitation and extraction to obtain lignin [46]. Kamble et al. [47] reported the best condition of lignin precipitation used acetic acid at 9 pH, temperature $50^{\circ}C$ for maximum yield, as shown in Figure 16.
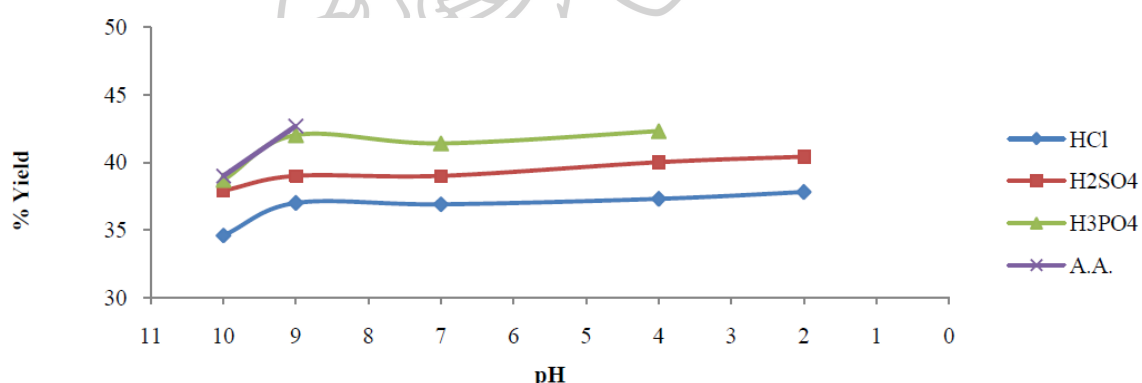


Figure  16 %Yield of black liquor by different acids [47].

3.2 PLA Casting Films

PLA can be molded by extrusion, injection molding, injection stretch blow molding, casting, blown film, thermoforming, foaming, blending, fiber spinning, and compounding [48]. The preparation PLA films can be performed in multiform, typically using solvent-casting film preparation method [49]. Youngjae Byun et al. [50] reported PLA films using methylene chloride: acetonitrile based-solvent had the highest

crystallinity, which results was brittle in mechanical properties, while the use of chloroform and methylene chloride was less crystalline, resulting in ductile mechanical properties, as shown in Figure 17.
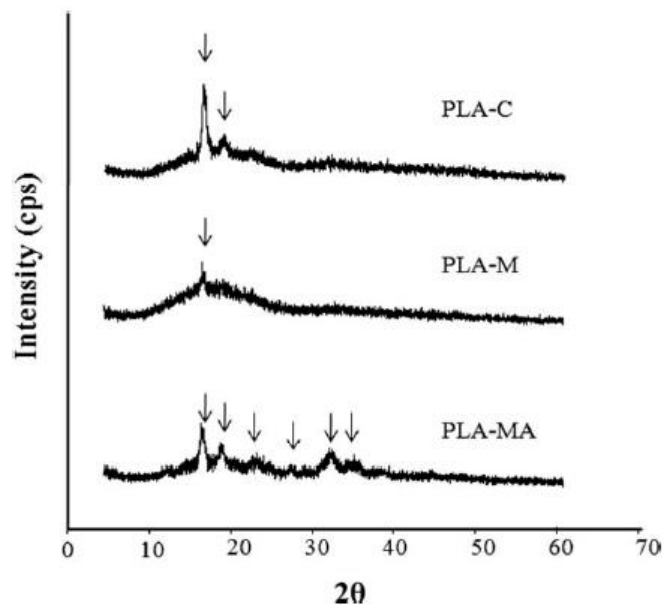


**Figure 17** X-ray diffraction of the different based-solvent PLA films [50].

## 3.3 PLA/Lignin Composite Films

The use of lignin as a filler in polymer provides a lot of enhancements such as anti-oxidation and UV absorption, thus increasing the value of the product [51]. Xiang Li et al. [52] reported PLA did not have UV protection because it was translucent in both the visible and UV ranges, but when added lignin it reduced the light transmittance in the UV range. Weijun Yang et al. [53] reported PLA composite films were reduced optical transparency when increased LMP contents and retain almost 100 wt% of UV-C and UV-B irradiation according to Figure 18. Shiv Shankar et al. [54] reported the aromatic ring in the lignin structure helps to absorb light during ultraviolet region. Yong Qian et al. [55] reported lignin containing methoxyl group to help the substance to prevent UV better. Tatiana Dizhbite et al. [56] reported lignin has a phenyl propane structure which was able to interact with DPPH, and its antioxidant performance

depended on the rate of hydrogen atoms from the phenyl group and the stability of the resulting radicals. Sandra Domenek et al. [6] reported the neat PLA did not change but the least residual DPPH$^{\circ}$ is lignin 10 wt% film which down to 42% of residual DPPH$^{\circ}$ as detailed in Figure 19.
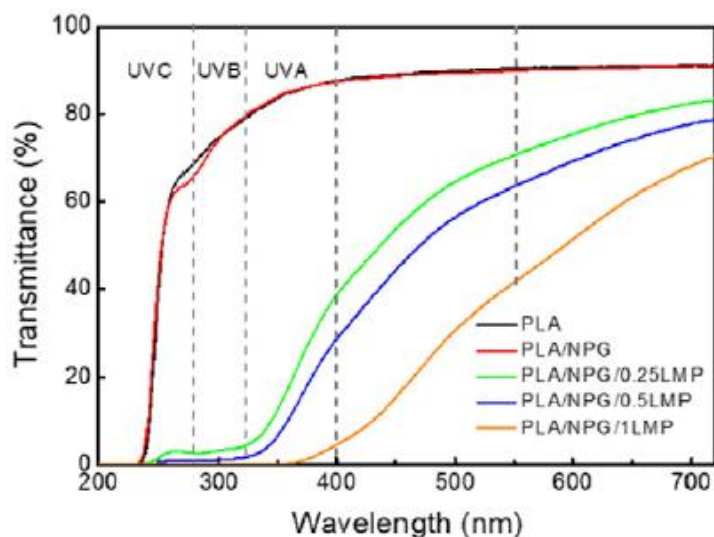


**Figure   18** UV-Vis spectra of neat PLA and PLA composite films [53].
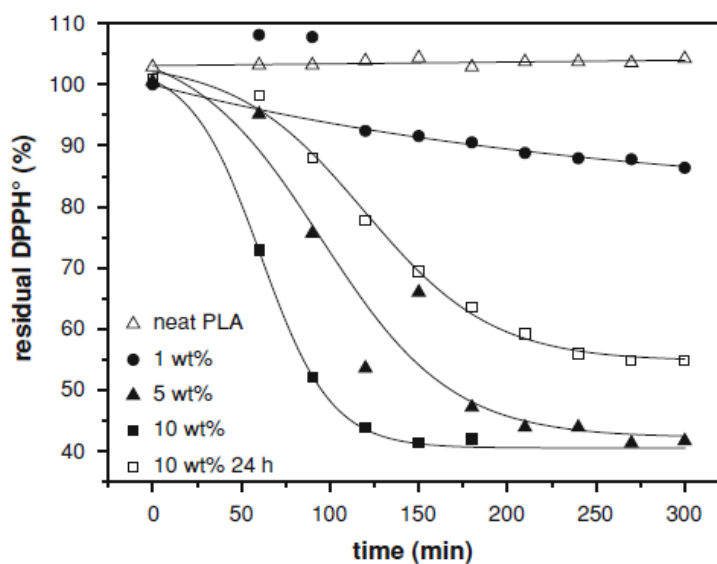


**Figure   19** The free radical DPPH$^{\circ}$ of neat PLA, various of lignin-PLA in methanol/DPPH$^{\circ}$ solution and a second time 10 wt% 24 h lignin-PLA after being extracted in ethanol/water (95/5 v/v) [6].

## 3.4 Beeswax Coating

PLA has some limitations in use due to its relatively low resistance to oxygen and water vapor permeability [57]. Film development using edible coatings is a combination of polymer matrix and hydrophobic components where the coating blocks moisture transfer [58]. Mônica Oliveira Reis et al. [59] reported that trays of thermoplastic starch (TPS)/PLA blends film coated with beeswax demonstrated WVP ranging from $7.9 \times 10^{-11}$ to $0.2 \times 10^{-11}$ g/m.s.Pa (reduce to 65%, when compared with uncoated) because beeswax is more hydrophobic properties, as shown in Figure 20.
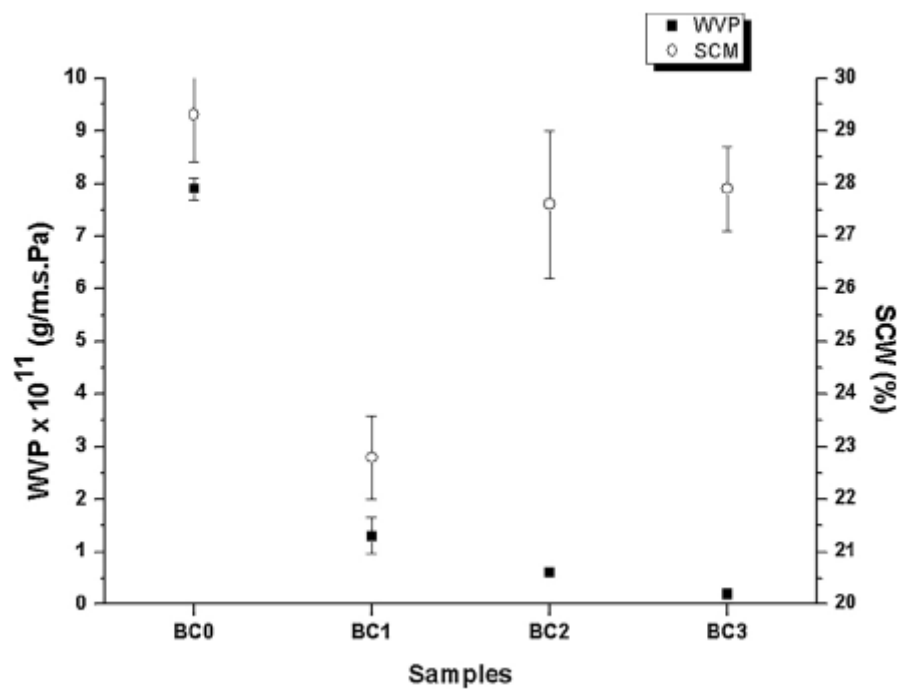


**Figure 20** Effect of the water vapor permeability(WVP) and the solubilization capacity in water(SCW) for the trays [59].

It was considered that dipping in hexane removed the low MW components and also able to enhance the molecular arrangement of conjugated polymer thin films effectively [60]. Manlin Tan et al. [61] reported that two solutions were compared: FDTS/n-hexane and FDTS/Vertrel XF solution when the film was dipped in FDTS/n-

hexane solution, the CA and roughness values were higher than FDTS/Vertrel XF solution because rather rough morphology, as shown in Figure 21-22.
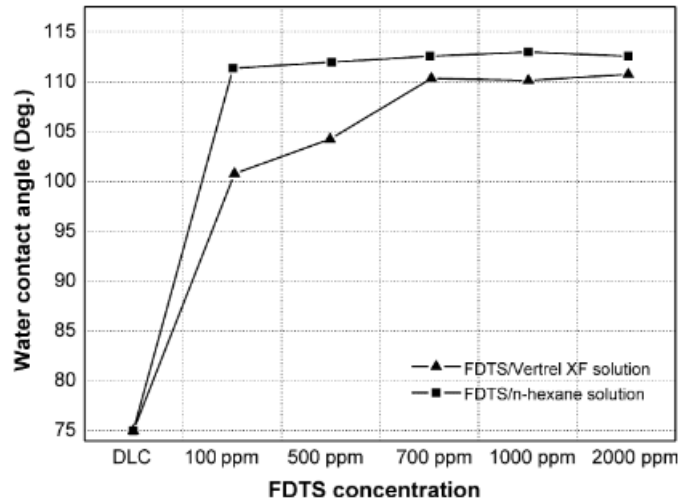


Figure  21 The changing in the water contact angle with the concentration of FDTS/n-hexane and FDTS/Vetrel XF [61] .
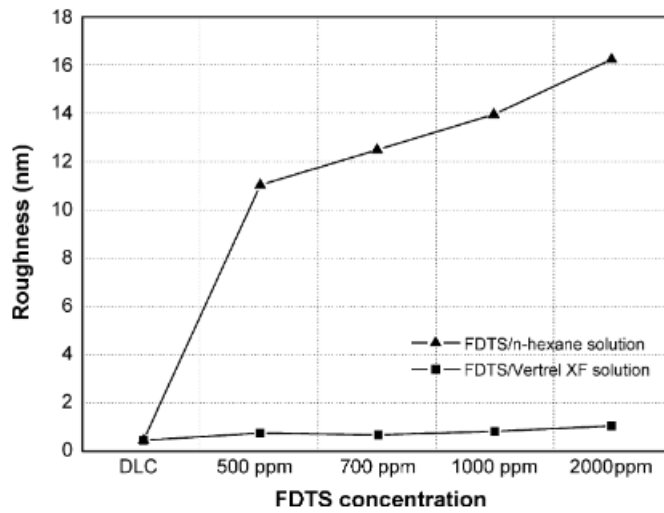


Figure  22 The correlation between surface roughness and solution concentration FDTS/n-Hexane and FDTS/Vetrel X [61].

# CHAPTER 4

# METHODOLOGY

## 4.1 Materials

### 4.1.1 Poly(Lactic Acid) (PLA)

PLA (commercial name is Ingeo biopolymer 2003D) was produced by Nature Works LLC. PLA has melt flow index and specific gravity of 6 g/10 min and 1.24 g/cm$^3$ respectively.

### 4.1.2 Lignin

At 50°C, 100 ml of black liquor was stirred and 1 ml of acetic acid was dropped at a rate of 1 ml/min. Acetic acid at 50°C is the ideal temperature for achieving a high percent yield of lignin [47]. The mixture was then blended for 10 minutes, and the pH was 9. It was left overnight after measurement. Finally, the lignin particles were removed using a Buchner funnel and Whatman No 41 filter paper before the pH was adjusted to neutral. The pH of the precipitation has no effect on the yield percentage or purity. [46].

### 4.1.3 Beeswax

Beeswax was imported from Germany where it was purified. It is insoluble in water and insoluble in cold alcohol. Beeswax has a melting point of 62-64°C. The relative density at 15°C is 0.958-0.970 g/cm$^3$.

## 4.2 Sample Preparation

### 4.2.1 Preparation of PLA films

PLA 1.2 g was dissolved in 20 ml chloroform and agitated at room temperature until completely dissolved. After that, the solution was placed in a petri dish and kept at room temperature, covered with foil, until the solvent had completely evaporated. For 24 hours, the films were continuously dried in a 60°C oven. PLA was mixed with lignin

concentrations of 0.5, 1, 3, and 5 phr. PLA/lignin composite films were created in the same way that PLA films were.

### 4.2.2 Preparation of PLA/lignin films

Lignin 0.5, 1, 3 and 5 phr was mixed with PLA and apply everything as in PLA films. After complete solution was pour on a petri dish and leave complete evaporated as same as preparation PLA films.

### 4.2.3 Preparation of PLA/lignin films coated with beeswax by dipping coating

The prepared PLA/lignin films were coated beeswax by dipping in beeswax at the concentrations of 5, 10, 15 and 20 wt%. The beeswax was melted in hexane at 70°C, then the film was dipped for 2 minutes [9, 62]. After that, the coated film was dried overnight at room temperature.

### 4.2.4 Preparation of PLA/lignin films coated with beeswax by rod coating

The prepared PLA/lignin film was coated with beeswax, which used a groove size of 40μ. Beeswax 10g was melted at 70°C. When completely melt, the solution was pour onto the prepared film and use groove size at 12, 24, 40 and 50μ to evenly spread. Then leave it until the coating is completely dry.

## 4.3 Sample Characterization

### 4.3.1 Scanning Electron Microscopy (SEM)

SEM (MIRA3, TESCAN, Czech) was used to observe the morphology and distribution of lignin particles in the PLA matrix and beeswax coating, as shown in Figure 23. All specimens were sputter coated with gold and were detected by Secondary electrons (SE) and Backscattered electron (BSE) with an accelerating voltage of 5 kV.

**Figure 23** Scanning electron microscopy (MIRA3, TESCAN, Czech).

**4.3.2 Universal Tensile Testing**

Universal tensile testing (Tinius Olsen THE 1000N universal testing machine) was used to observe the mechanical properties of the composite films following ASTM D882, as shown in Figure 24. The specimen size was 50 x 15 mm$^2$ and gage length 50 mm. The tensile test was performed at a crosshead speed of 5 mm/min and preload 0.01 N. The results obtained represented the average triplicate specimens.



**Figure 24** Universal tensile testing (Tinius Olsen THE 1000N universal testing machine).

### 4.3.3 Thermogravimetric analysis (TGA)

TGA (SDT Q600, TA Instruments, UK) was used to characterize thermal properties of the composite films, as shown in Figure 25. The composite films were cut into small pieces of a mass range between 10-20 mg then it placed in aluminum pans. The measurement was carried out in a nitrogen atmosphere at a temperature range of 50-600°C at a heating rate of 10°C/min.



**Figure  25** TA Instruments (SDT-Q600, UK).

### 4.3.4 Fourier Transform Infrared Spectroscopy (FTIR)

FTIR (Nicolet iS5 spectrometer) was used to measure the chemical structures and functional groups of the samples in a range from 400 to 4000 cm$^{-1}$ as shown in Figure 26.



**Figure  26** TA Instruments (SDT Q600, TA Instruments, UK).

### 4.3.5 X-Ray Diffraction (XRD) Spectroscopy

XRD (D8 advance, Bruker, USA) operates at 40 kV and 30 mA with a wavelength of approximately 0.154 nm. It was used to examine the sample diffraction pattern. The sample was scanned from $4^{\circ}$ to $80^{\circ}$ with a step size of $0.02^{\circ}$.

### 4.3.6 Ultraviolet-Visible Spectroscopy (UV-Vis)

Investigation of film blocking properties, the specimen is cut into 2x2 $cm^{2}$ rectangle and placed in a spectrophotometer test cell directly and air was used as a reference. The absorbency of the film was recorded in the range of 200-800 nm using UV-Vis spectrophotometer (VARIAN, Cary 5000), as shown in Figure 27. UV-Vis spectrophotometer (T92+, PG Instruments, UK) was measured UV absorbance at 518 nm to determine the DPPH scavenging activity of the composite films, as shown in Figure 28.
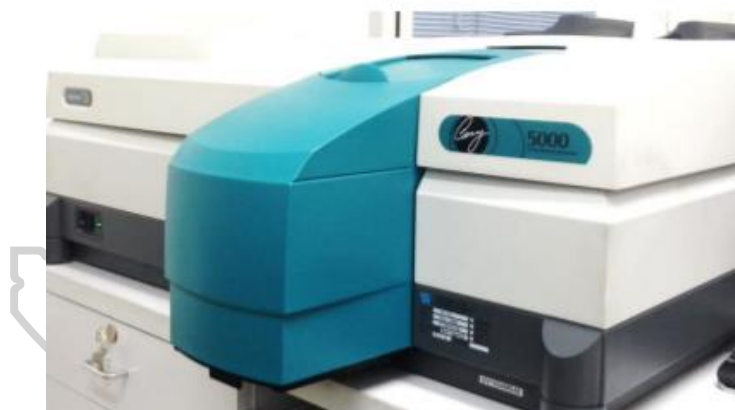


**Figure 27** UV-Vis spectrophotometer (Cary 5000, Varian, USA).



**Figure 28** UV-Vis spectrophotometer (T92+, PG Instruments, UK).

### 4.3.7 Water Vapor Transmission Rate (WVTR)

Water vapor transmission was measured using MOCON Permatran-W Model 398 as shown in Figure 29. The measuring the transient water vapor transmission of a polymer film by directing the liquid water to either side to producing saturated vapor and investigate the water vapor transmission rate (WVTR) as a function of time.



**Figure 29** MOCON Permatran-W Model 398.

### 4.3.8 Water Contact Angles (WCA)

The water contact angles were measured with 20 μL deionized water using DinoliteCapture 2.0 software (Dino-Lite & Dino-Eye). The average contact angle value of water was obtained by measuring at five different positions for the same sample.

### 4.3.9 Antioxidant Activity Assay

The antioxidant activity of the films were assessed by DPPH (2,2-diphenyl-1-picrylhydrazyl) free radical scavenging assay. Cutting the film into small sizes around weight 0.2 g add with methanol 4 ml and let it at room temperature for 24 hours. The extract was taken 1ml, added to the DPPH solution in methanol (0.0634 mM) and kept in

a dark place at room temperature for 30 min. The following, the absorbance was measured 518 nm.

The reduction in radical scavenging activity (%RSA) is calculated as follows:

$$\% \text{ RSA} = 100 - \left( \frac{A_{blank} - A_{sample}}{A_{blank}} \right) \times 100 \tag{2}$$

$$\text{Inhibition } \% = \left( \frac{A_{blank} - A_{sample}}{A_{blank}} \right) \times 100 \tag{3}$$

Where $A_{blank}$ is the absorbance of the DPPH solution and $A_{sample}$ is the absorbance of the DPPH solution containing the extracted film.
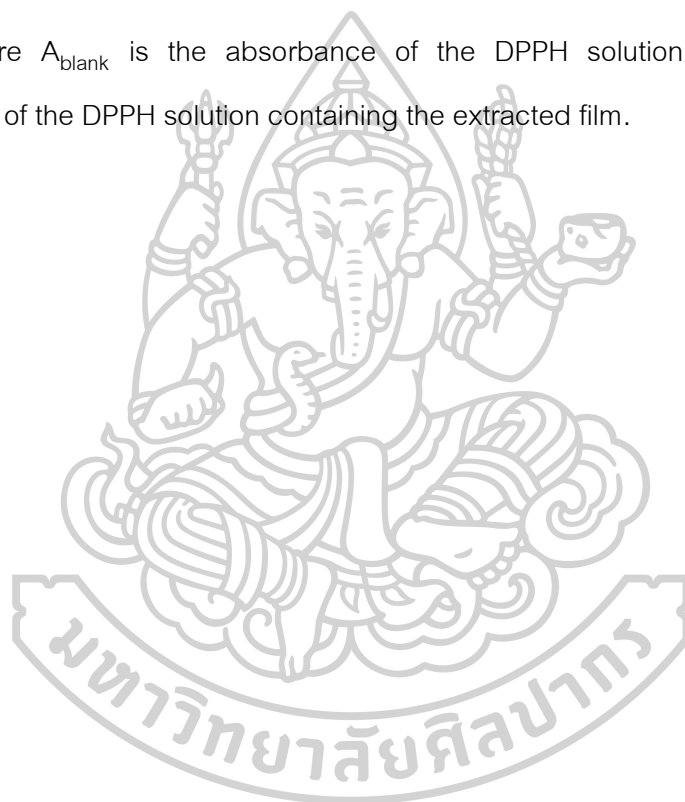
# CHAPTER 5

# RESULTS AND DISCUSSION

## 5.1 Characterization of the Lignin

The production of kraft pulp produces black liquor as a by-product, which contains lignin. To obtain the lignin, black liquor was precipitated with organic acids. Figure 30(a-b) shows a SEM image of precipitated lignin with a particle size of about 15 µm. The structure of lignin did not show cavities and cracks when precipitated with an organic acid, acetic acid. Precipitation lignin has increased cavities and cracks, which will affect the plastic. This can cause the plastic from the internal cavity to deform [63]. The occurrence of cavitation can support the inference that organic acids modify lignin in the kraft during precipitation. Therefore, the extracted lignin does not result in the polymer deforming.



(a) 1000x magnification                    (b) 10000x magnification
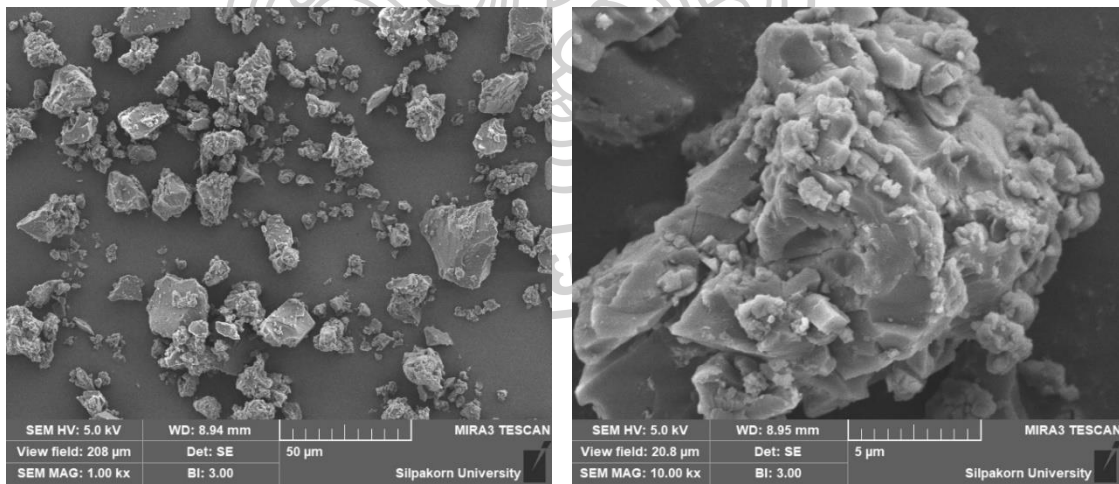
Figure  30 SEM micrographs of the lignin particles.

The lignin was precipitated that is type L lignins (Guaiacyl-Syringyl lignins). Lignin mainly contain guaiacylpropane unit, syringylpropane unit, some p-hydroxyphenylpropane units. As shown in Figure 31, FTIR spectroscopy was used to compare functional groups of lignin structures to the lignin standard. The peak at 3400 cm$^{-1}$ represents the OH stretching vibration in aromatic and aliphatic OH groups, and the intensity of this peak varies depending on the process of lignin precipitation. The peaks at 2938 cm$^{-1}$ and 2850 cm$^{-1}$ are caused by CH stretching in aromatic methoxyl groups as well as methyl and methylene side chain groups [64]. The fingerprint of lignin is approximately 1800-900 cm$^{-1}$ [63]. The extracted lignin was compared with standard lignin. A common peak at approximately 1600, 1525, 1440, 1217 and 1034 cm$^{-1}$, which generalizes the monomers of the guaiacyl and syringyl backbone of the lignin particles, are observed.
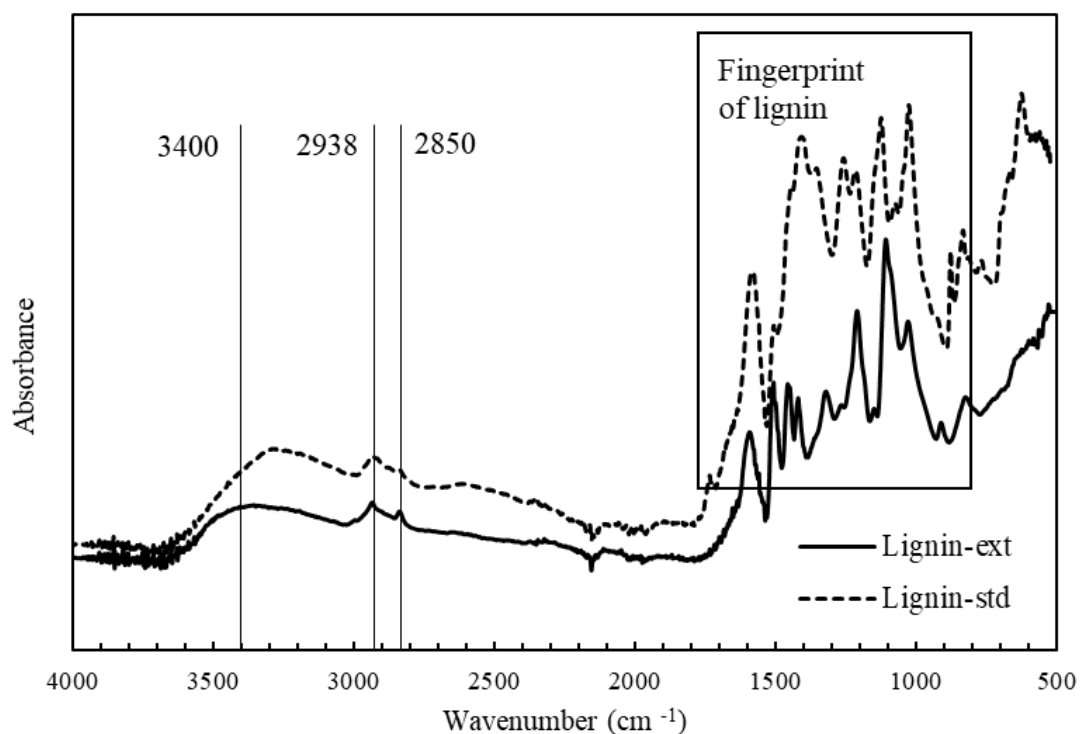


**Figure 31** FTIR spectra of standard lignin and precipitated lignin from the black liquor.

5.2 Characterization of PLA/Lignin Composite Films

    5.2.1 Morphology

    SEM is used for analysis of the surface and the distribution of filler in polymer matrix [65]. The images of SEM indicate PLA, PLA/lignin 0.5, PLA/lignin 1, PLA/lignin 3 and PLA/lignin 5 for top bottom and cross-section surface as illustrated in Figure 32(a-o). Upon referring to the top surface of the film, increasing the lignin content causes the surface roughness to rise. On the upper surface, the SEM picture reveals a considerable amount of lignin and agglomerate particles [65]. The distribution and interface between PLA and lignin may be seen on the bottom surface and cross-section surface. Figure 32(e,k) shows an increase in rough voids at 0.5 and 3 phr at the bottom surface, compared to neat PLA in Figure 32(b). Because of the smaller lignin distribution size and better interface, PLA/lignin films at 1 and 5 phr exhibited fewer gaps, as illustrated in Figure 32(h,n). The lignin cross-sectional surfaces at 0.5 phr and 3 phr in Figure 32(f,l). It is clearly observed that large agglomerates of lignin and forming a void are found in the PLA matrix. For the addition of lignin at 1 phr and 5 phr, it was found that lignin was well distributed in the PLA matrix, which reduced the internal voids. As a result, if high-charging lignin in the PLA matrix does not improve the mechanical characteristics of PLA, then an appropriate amount of lignin can be added to the interface. Lignin's outstanding dispersion quality can help improve mechanical qualities.

|                | Top | Bottom | Cross-section |
|---|---|---|---|
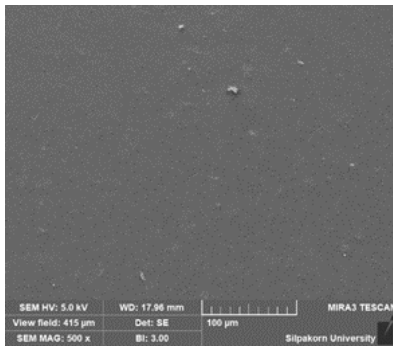


(a) PLA 500x magnification
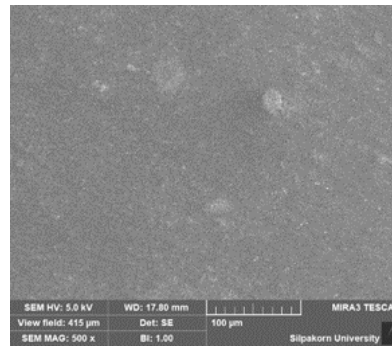


(b) PLA 500x magnification
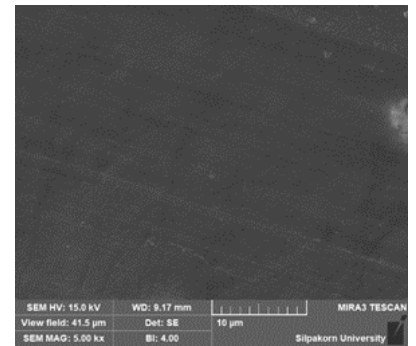


(c) PLA 5000x magnification
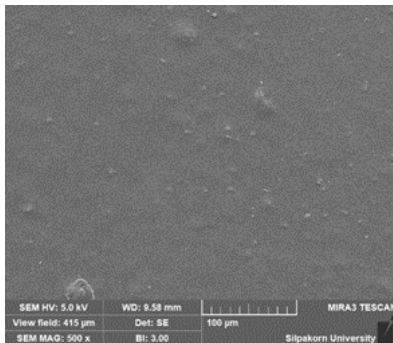


(d) PLA/lignin (100/0.5) 500x magnification
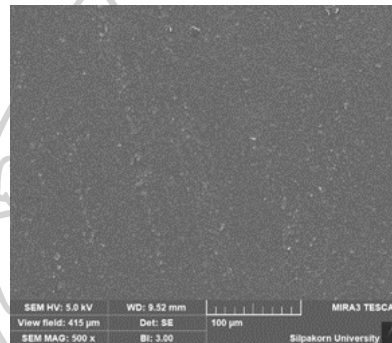


(e) PLA/lignin (100/0.5) 500x magnification
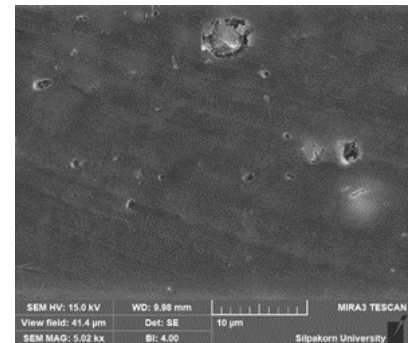


(f) PLA/lignin (100/0.5) 5000x magnification
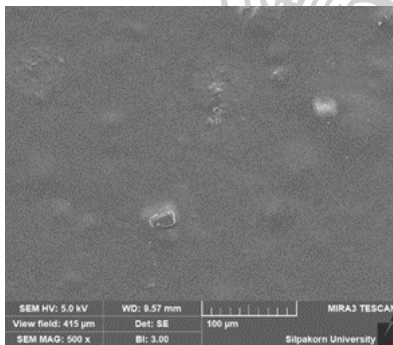


(g) PLA/lignin (100/1) 500x magnification
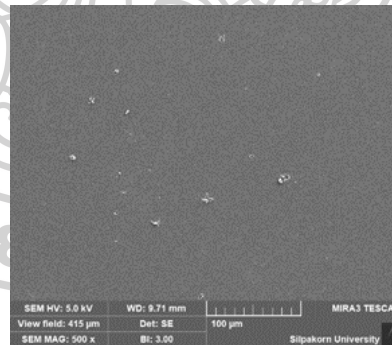


(h) PLA/lignin (100/1) 500x magnification
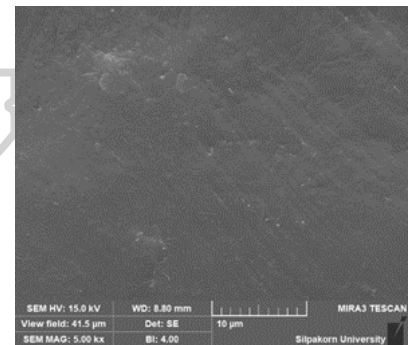


(i) PLA/lignin (100/1) 5000x magnification

| Top | Bottom | Cross-section |
|---|---|---|



(j) PLA/lignin (100/3) 500x magnification



(k) PLA/lignin (100/3) 500x magnification



(l) PLA/lignin (100/3) 5000x magnification



(m) PLA/lignin (100/5) 500x magnification



(n) PLA/lignin (100/5) 500x magnification



(o) PLA/lignin (100/5) 5000x magnification
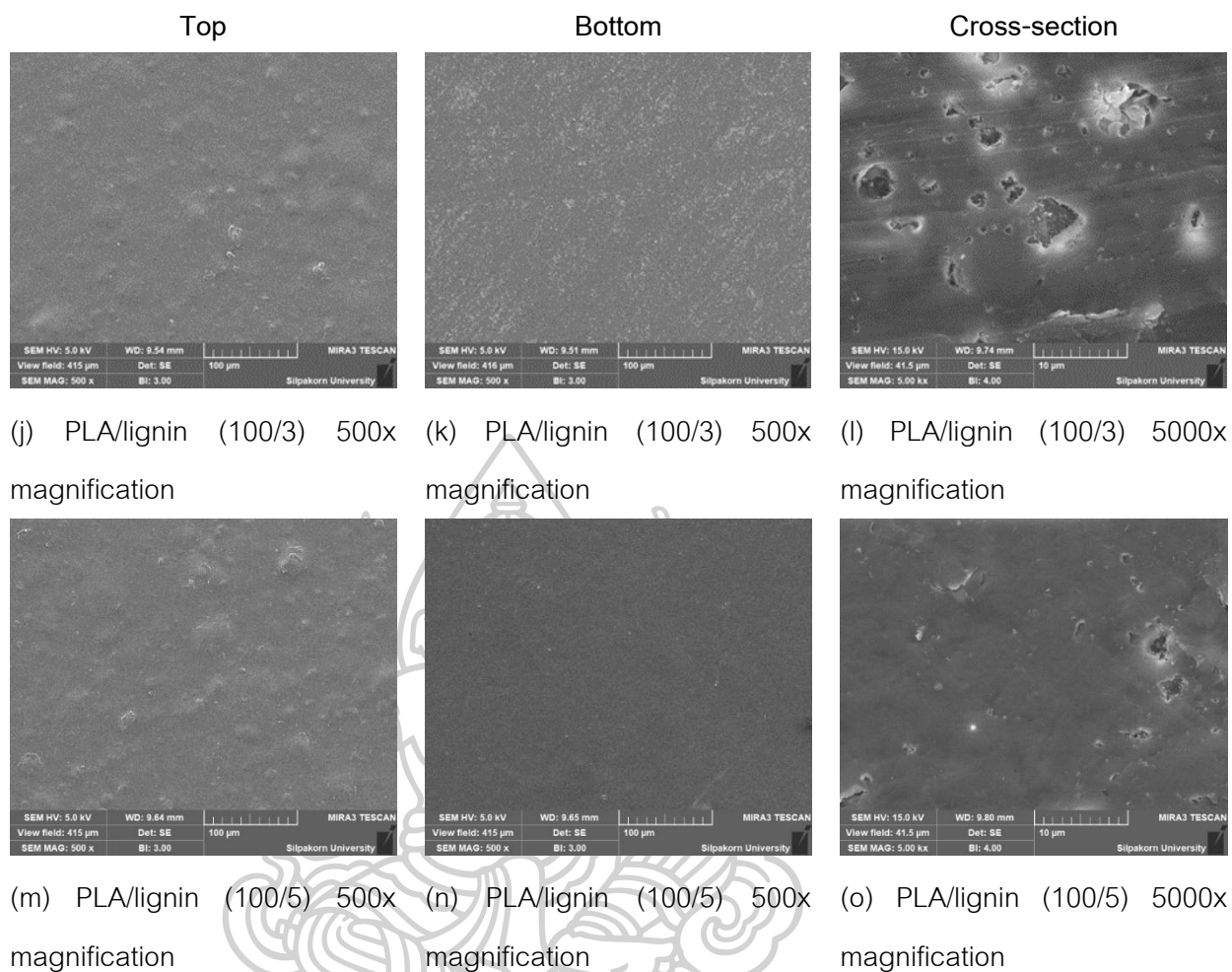
**Figure 32** SEM micrographs of PLA and PLA/lignin at different lignin contents.

### 5.2.2 FTIR analysis

FTIR spectroscopy is used to investigate the interactions between PLA and lignin. Neat PLA shows a characteristic peaks at 2995, 2946, 1753, 1455, 1384, 1269-1045, 921 and 870 $cm^{-1}$, as show in Figure 33 [66] [67]. The peak at 2995 and 2946 $cm^{-1}$ were -CH stretching for $CH_3$ asymmetric and $CH_3$ symmetric, respectively. The strong absorption at 1753 $cm^{-1}$ was assigned to the C=O stretching vibration of ester groups. The bands at 1455 and 1384 $cm^{-1}$ were ascribed the C-H symmetric and C-H asymmetric deformations, respectively. The absorption bands corresponding to C-O

stretching at 1269-1045 cm$^{-1}$. Figure 34 show two shoulders at 1753 cm$^{-1}$ and 1748 cm$^{-1}$ when the addition of lignin 0.5, 1, 3 and 5 phr was observed smoothly with increase contents. The presence of primary band separation associated with carbonyl stretch vibration may be due to low interaction between the lignin of OH group and PLA of C=O group [66]. The vibration band at 921 cm$^{-1}$ presents a crystalline and the -C-OH bending of the carboxylic acid groups in PLA, as shown in Figure 35 [68] [69]. The bands at 756 and 870 cm$^{-1}$ corresponded to -C-C- stretching crystalline phase and -C-C- stretching amorphous phase of PLA, respectively, as shown in Figure 35 [68] [70]. Examination of the FTIR spectra of all composite films showed that the addition of lignin had no significant influence on the PLA characteristic bands [66].
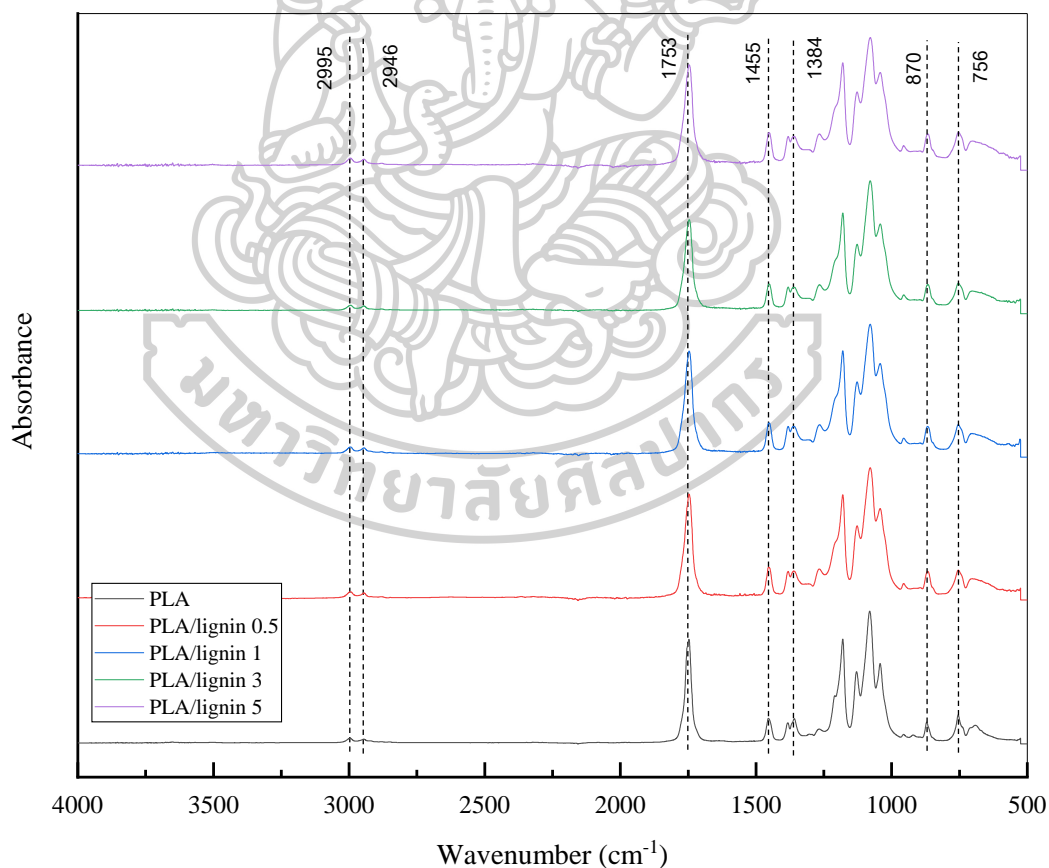


**Figure 33** FTIR spectra of neat PLA and PLA/lignin composites.
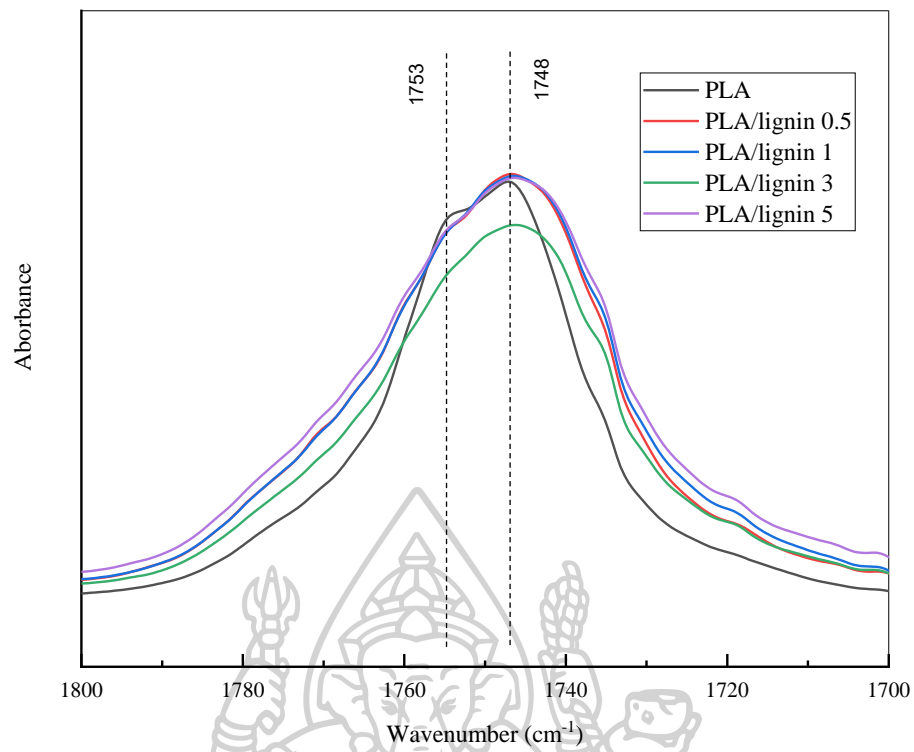
**Figure 34** FTIR spectra of neat PLA and PLA/lignin composites at 1753 and 1748 cm⁻¹.
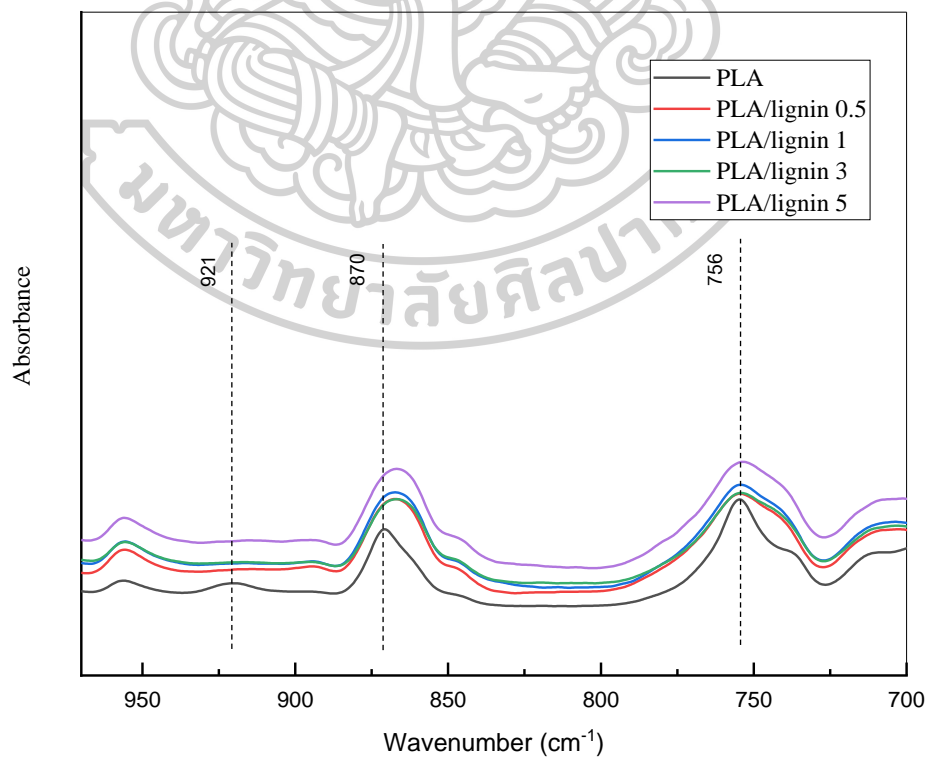


**Figure 35** FTIR spectra of neat PLA and PLA/lignin composites in range 970-700 cm⁻¹.

### 5.2.3 XRD analysis

The X-ray diffraction (XRD) analysis is used to study the crystalline characteristics of the composite films. The results of XRD are demonstrated in Figure 36 for neat PLA and PLA/lignin composite films. The main diffraction peaks are observed at $2\theta$ = 16.5° and 18.3° for neat PLA. The addition of lignin leads to an increase in the intensity of the crystalline peaks, reflecting that lignin acts as by a nucleating agent in promoting the crystallinity of the PLA matrix. This is likely a result of the interaction between the hydroxyl or carbonyl functional groups of lignin that induce hydrogen bonding and hence crystal formation. However, a high nucleating agent interferes with molecular chain alignment, resulting in low crystallinity [71]. As lignin is an amorphous matter. The amorphous phase is increased in the composite film due to the addition of lignin [72] .

The width-at-half-height of the crystal-peaks were widened with the addition of lignin, reflecting the lower regularity or quality of the crystal domains. The broadest peaks, with the least order and crystallinity, were observed when 1  phr lignin was added. This likely indicates high compatibility of the lignin in the PLA matrix, leading to the interference with its crystal formation.

The crystallite size was calculated by using the Scherrer equation, as reported in Table 1. PLA exhibited a larger crystallite size at 10.69 nm due to a sharper peak than PLA/lignin 1 (crystallite size at 9.99 nm). The peaks become sharper and the crystallite size increase, indicating a more organized structure [73].
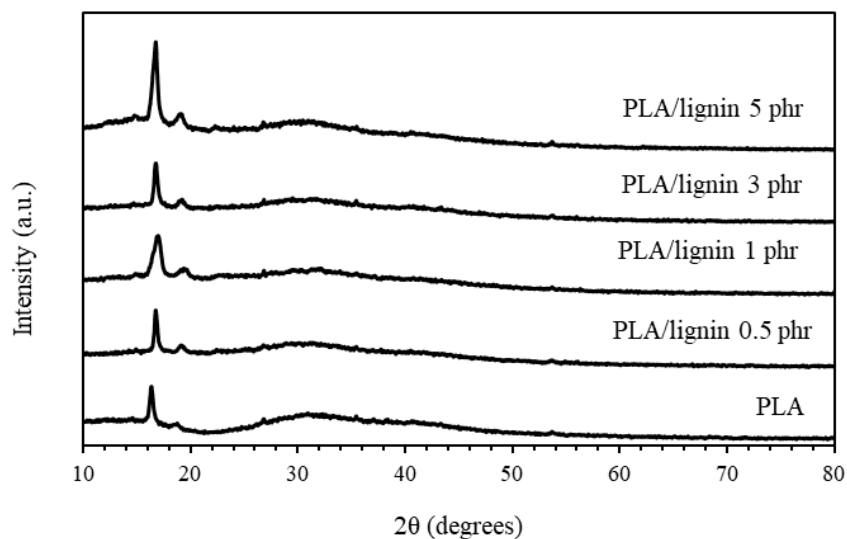
Figure 36 X-ray diffraction patterns of PLA and PLA/lignin composite films.

Table 1 The crystallite size calculated from XRD.

| Sample | Crystallite size (nm) |
| --- | --- |
| PLA | 10.69 |
| PLA/lignin 0.5 phr | 22.96 |
| PLA/lignin 1 phr | 9.99 |
| PLA/lignin 3 phr | 19.68 |
| PLA/lignin 5 phr | 14.06 |

### 5.2.4 Mechanical properties

The effect of lignin distribution on small (<150 µm) was a larger positive correlation with lignin dispersion than large (355–500 µm), resulting in a very significant negative [74]. This enhances stress transfer by reducing the amount of empty space on the entire surface. The effects of the lignin contents on stress-strain curves, tensile strength, Young's modulus and elongation at break are examined by tensile testing, as reported in Figure 37-40. Figure 37 depicts the stress-strain curves of PLA and PLA/lignin films with various lignin contents. As the lignin content increased, the stress

level reduced. This suggests that the force of PLA/lignin decreases as the lignin level rises. The end result was achieved by applying a modest amount of stress to the film, causing it to tear readily. In comparison to neat PLA, the strain at break reduced as the lignin level increased. Because of the improved distribution size and interface as seen in SEM images, the PLA/lignin 1 phr exhibits the highest percent strain. When considering the beginning of the deformation process between lignin and PLA, the craze shape may be torn, which gradually rips to absorb energy better [75]. As a result, as shown in Figure 32(h), lignin acts as a nucleus formation agent as well as a hardening agent to raise the density of the PLA matrix. Figure 38 shows the tensile strength of PLA and PLA/lignin films at various lignin concentrations. The tensile strength of the material dropped as the lignin percentage increased. This shows that the PLA/lignin was weaker than neat PLA. It has also been linked to lignin incorporation at increased lignin content, which causes fissures in composite films [76]. Young's modulus of PLA and PLA/lignin at various lignin concentrations is shown in Figure 39. With increasing lignin content, the Young's modulus fell, indicating that the PLA/lignin was less stiff. Figure 40 depicts the elongation at break of a PLA/lignin composite; elongation at break was shown to be reduced with increasing lignin content, with the exception of the addition of lignin at 1phr. PLA/lignin 1 phr has the greatest elongation at break, meaning that it can stretch the longest before breaking.
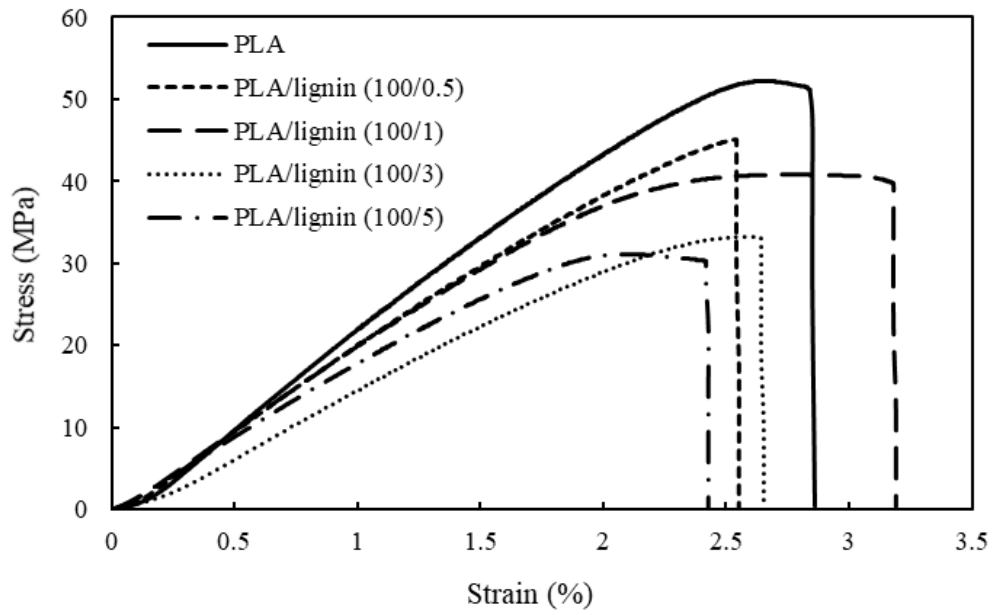
Figure 37 Stress-strain curves of PLA and PLA/lignin composite films.
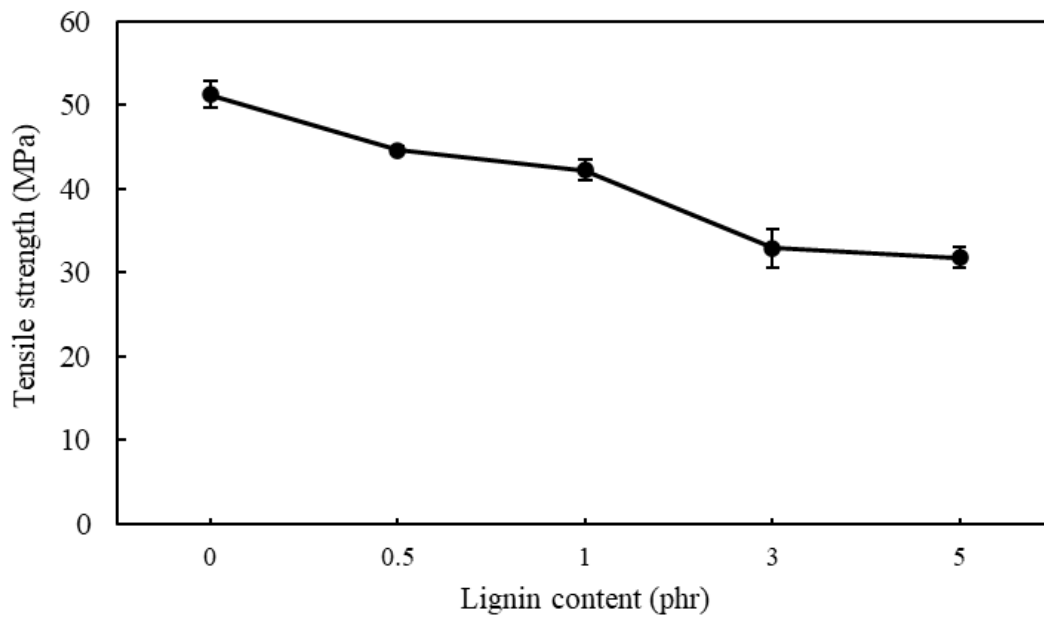


Figure 38 Tensile strength of PLA and PLA/lignin composite films.
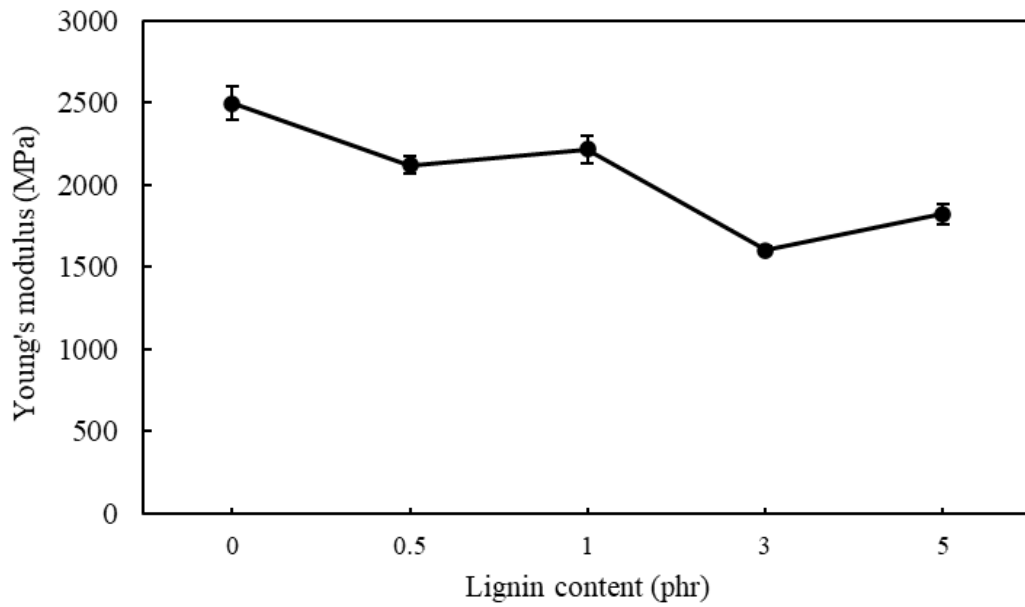
Figure 39 Young's modulus of PLA and PLA/lignin composite films.
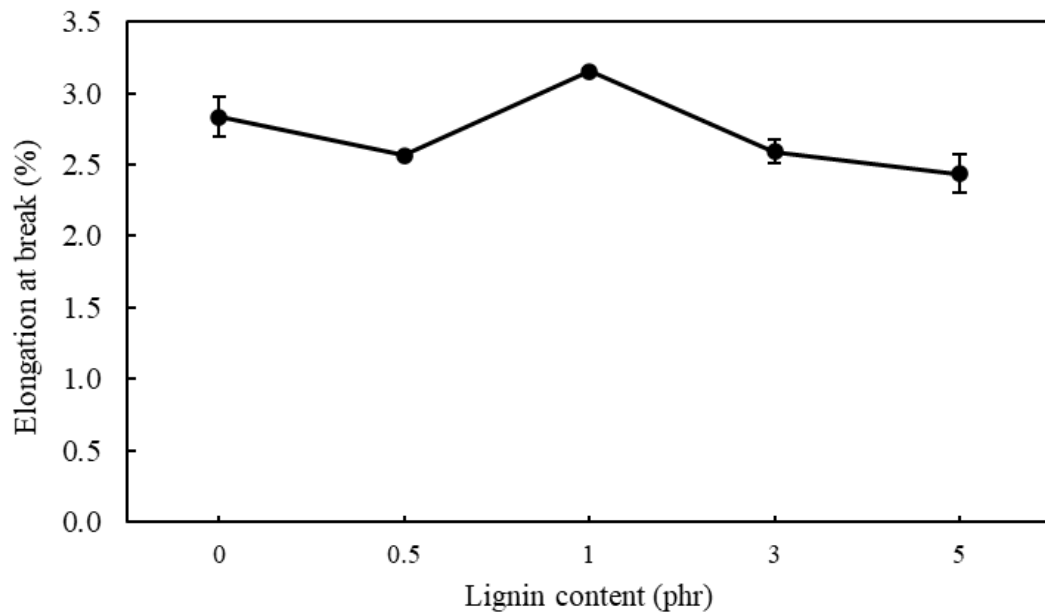


Figure 40 Elongation at break of PLA and PLA/lignin composite films.

### 5.2.5 Thermal properties

### 5.2.5.1 TGA analysis

Thermal analysis is the change in physical and chemical properties of a material that is observed by increasing temperature [77]. The thermal decomposition of neat PLA and PLA/lignin composite films, as shown in Figure 41, was studied by thermogravimetric (TG). The thermal degradation process of PLA and PLA/lignin show two steps of degradation. The first step of both samples had a little weight loss below $100 °C$ caused by evaporation of moisture [78]. The second step is the main degradation step in a temperature range around $300\text{-}500° C$. This is associated with the fragmentation of inter-units linkage [79]. In addition, improvements in the thermal stability of PLA and PLA/lignin can be observed by initial degradation ($T_{d5}$) and char yield, as shown in Table 2. The addition of lignin with an increased amount resulted an increased thermal stability, which can be clearly seen with the addition of lignin at 1 phr an initial decomposition temperature. The high initial degradation temperature is able to maintain the thermal stability than neat PLA. The high thermal stability of lignin is due to the presence of complex phenylpropanoid units consisting of aromatic phenyl groups. These aromatic structures are very stable. Furthermore, the presence of multiple hydroxyl groups contributes to their stability because unpaired electrons are also highly stable. It increases the stability of the aromatic structure and hinders electron rupture, which occurs only at high temperatures [80]. Besides, the yield of char in both samples at $600 °C$ increased with an increase lignin content due to carbon residue remaining from lignin.

### 5.2.5.2 DSC analysis

DSC analysis was used to determine the thermal behavior which measured glass transformation ($T_g$), cold crystallization ($T_{cc}$) and melting temperature ($T_m$) and final crystallinity of PLA and PLA with lignin particles [81]. The DSC thermograms of PLA and PLA/lignin with different content are demonstrated in Figure 42. The glass transition

behavior of PLA/lignin compared to neat PLA shows wider temperature range, approximately 60°C. It is clearly seen that the addition of lignin at 1 and 5 phr are formed by complex molecular structures leading to multiple relaxation phases within the same temperature range [82]. DSC scans reported that the PLA and PLA/lignin composites films had no effect on the melting temperature [83]. The melting point ($T_m$) and crystallinity of neat PLA and PLA/lignin composite films are presented in Table 3. No significant differences between the PLA and PLA/lignin composite films was observed. The crystallinity increased from 9.03% for neat PLA to around 10% of PLA/lignin. This is due to the increase in cold crystallization with the presence of lignin particles [84]. With the exception of PLA/lignin 1 and PLA/lignin 3 was decreased compared with neat PLA, which the resulted had a tendency in the same direction with morphology and mechanical properties.
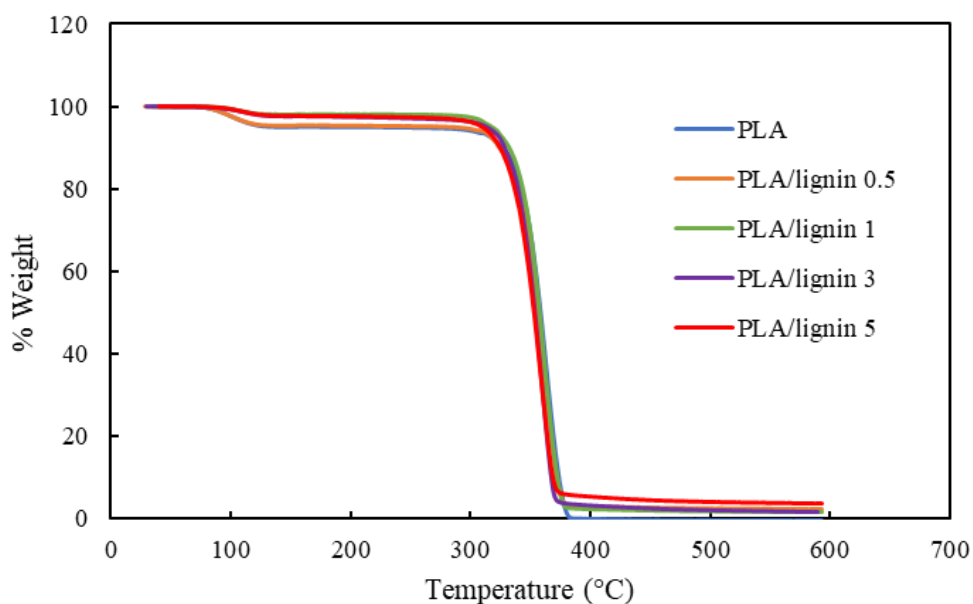


Figure  41 TG curves of neat PLA and PLA/lignin composite films.
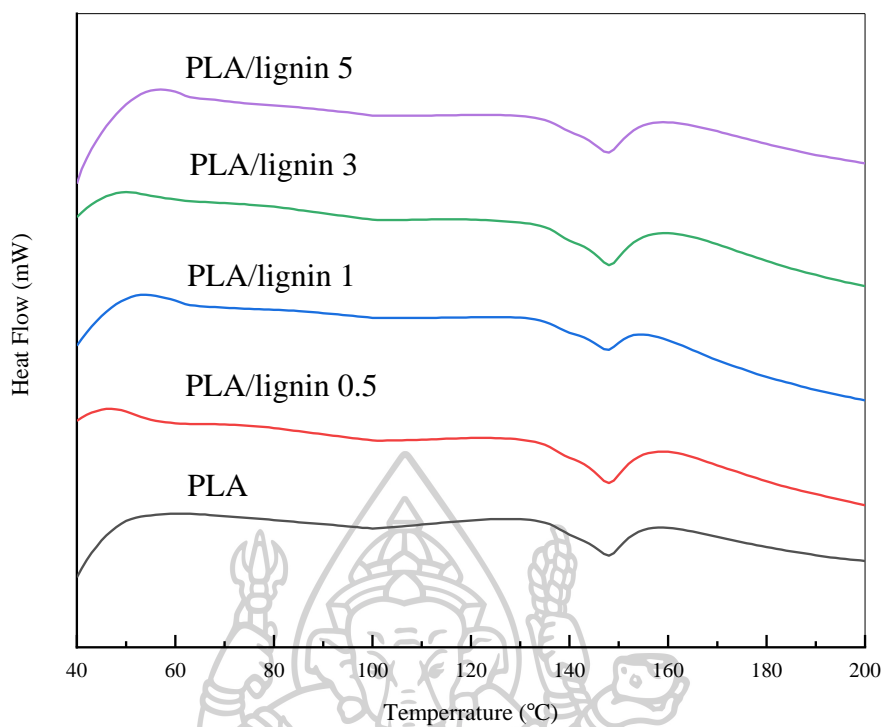
**Figure  42** DSC thermograms of PLA and PLA/lignin composite films.

**Table  2** The decomposition temperature of 5 %weight loss ($T_{d5}$) of neat PLA and PLA/lignin composite films.

| Sample | $T_{d5}$ (°C) | Char yield (%) |
|---|---|---|
| PLA | 138 | - |
| PLA/lignin 0.5 phr | 284 | 2.42 |
| PLA/lignin 1 phr | 318 | 1.52 |
| PLA/lignin 3 phr | 313 | 1.78 |
| PLA/lignin 5 phr | 310 | 3.62 |

Table 3 DSC analysis of neat PLA and PLA/lignin composite films.

| Sample | $T_m$ (°C) | Crystallinity (%) |
|---|---|---|
| PLA | 147.82 | 9.03 |
| PLA/lignin 0.5 phr | 147.77 | 10.41 |
| PLA/lignin 1 phr | 147.31 | 7.04 |
| PLA/lignin 3 phr | 147.90 | 11.44 |
| PLA/lignin 5 phr | 147.61 | 9.44 |

### 5.2.6 Optical properties

UV absorption is important for films used in food packaging [85]. PLA light transmittance was studied in two wavelength ranges: visible (400-800nm) and UV (250-400nm) [84]. The phenol hydroxyl groups in lignin can produce discoloration when exposed to UV radiation. Phenoxyl radicals are formed, which are partially oxidized to quinones. Quinones, on the other hand, are capable chromophores, and their light oxidizing into the aliphatic acid structure causes lignin decolorization [86]. After coming into contact with a sunbeam, this phenomenon has the potential to increase UV blocking capacities. The UV-Vis transmittance spectra of plain PLA and PLA/lignin composite films with varying lignin concentration are shown in Figure 43. The UV-Vis spectroscopy data demonstrate that tidy PLA has the highest light transmission. On the other hand, the lignin content with increased that decrease the light transmittance. It is evidenced that light transmittance decreases with increasing lignin, which means that lignin can greatly block the UV light region.
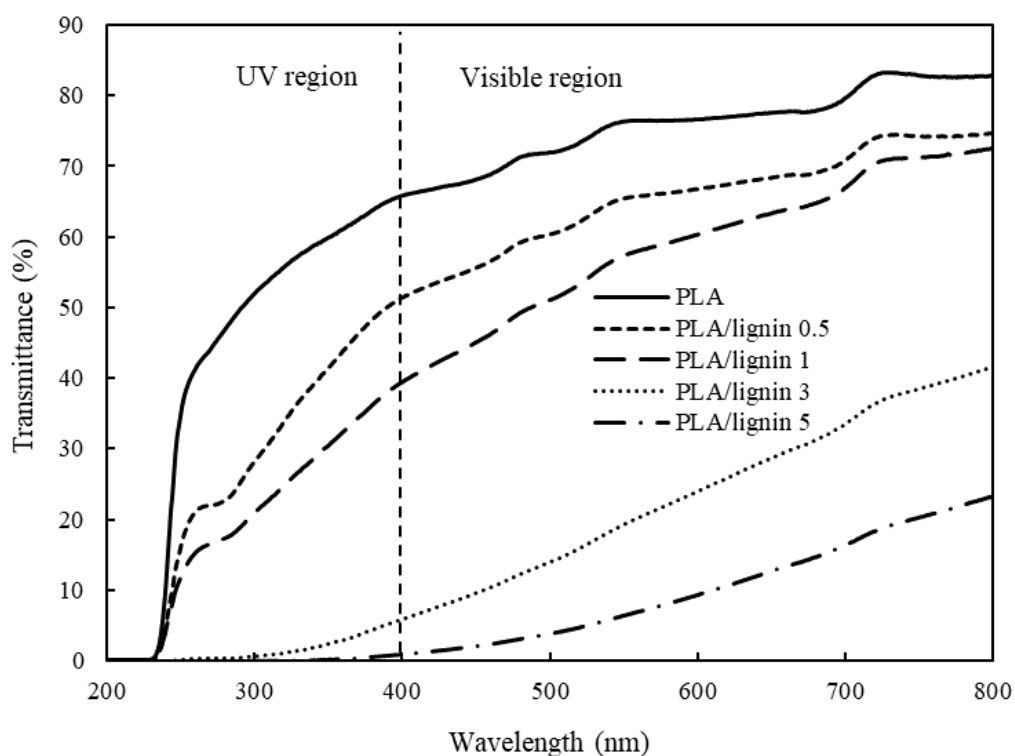
**Figure 43** UV-Vis transmittance spectra for PLA and PLA/lignin composite films.

### 5.2.7 Antioxidant activity

The definition of antioxidants is synthetic or natural chemicals added to products for preventing or slowing down the deterioration from oxygen in the air [87]. The lignin is considered a natural antioxidant in a class of polyphenols. It is known that the hydrogenation ability of phenolic compounds results in the scavenging ability of DPPH [88]. Cutting the film into small sizes around 5×5 mm$^2$ and weighing 0.2 g. Methanol 4 ml was added and the samples were extracted. The extract was taken 1 ml, and added to the DPPH solution in methanol. After that, the color change was observed and tested using a UV-Vis spectrophotometer at a wavelength of 518 nm. The DPPH scavenging can be seen by changing the color of the DPPH solution from dark purple to pale yellow indicating scavenging ability, as reported in Figure 44. The antioxidant activity of the lignin content added on PLA film that it was measured by evaluation of DPPH radical scavenging activity, as illustrated in Figure 45. The result follows the same trend as the

amount of lignin increases that also enabling scavenging activity with increase. It was clearly observed that the over addition of lignin at 1 phr was improved free radical inhibition by approximately 80% of inhibition. Consequently, the increasing lignin contents is consistent with the increased UV blocking performance. Also, the increasing potential of the UV-blocking and antioxidant association with phenolic hydroxyl groups reduce their antioxidant properties.
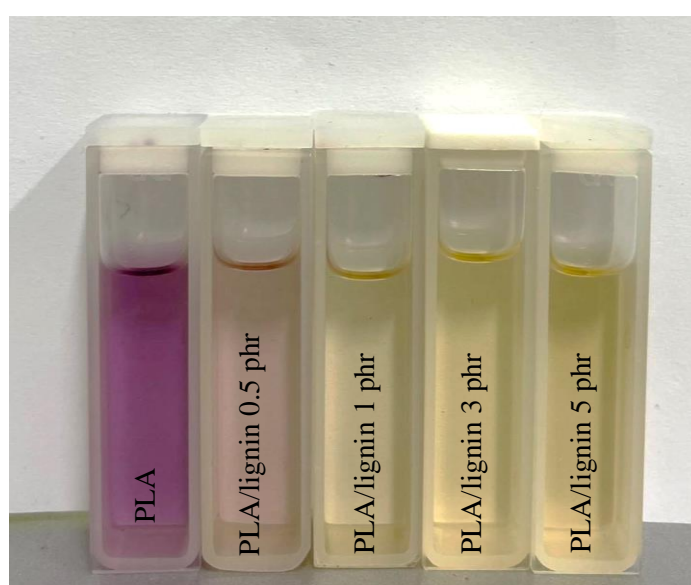


**Figure  44** Color change of DPPH solutions for PLA and PLA/lignin composite films.
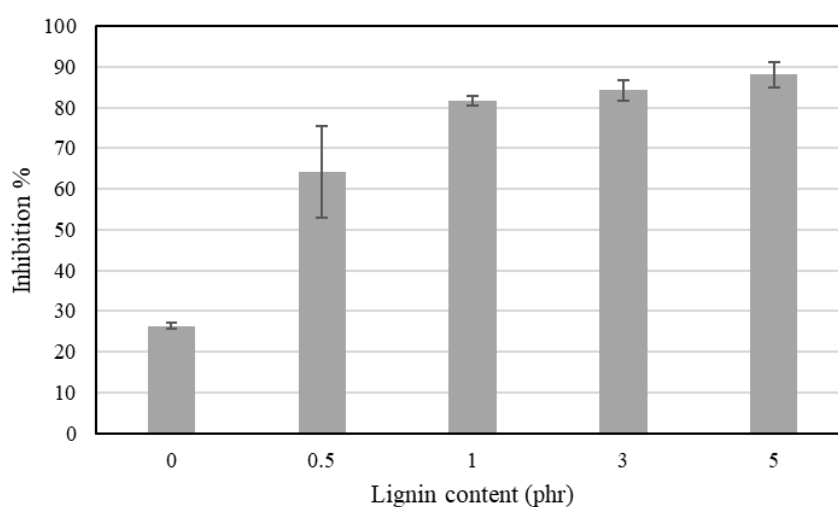
**Figure 45** The percent of free radical inhibition for PLA and PLA/lignin composite films.

### 5.2.8 Barrier properties

The main feature of food packaging materials is the ability to prevent or minimize water from penetrating the packaging materials. Therefore, the most common barrier property investigations are the water vapor transmission rate (WVTR) and the hydrophobicity, in terms of water contact angle (WCA) measurement [89].

#### 5.2.8.1 Water vapor transmission rate

The WVTR of the composite films is present in Table 4. The WVTR of neat PLA was 142.79 g/m$^2$-day. The PLA/lignin composite films at 1 phr was lower at 128.09 g/m$^2$-day. The decrease of WVTR is caused by the addition of lignin to increase the impermeable physical barriers in the PLA matrix. Then create tortuous paths and force water vapor to oscillate around them through a more tortuous path resulting in better water vapor diffusion protection performance [53] [90].

#### 5.2.8.2 Water contact angle

The hydrophobic effect of the film was studied when adding the lignin by measuring the water contact angle (WCA). Table 4 compares the WCA values of PLA and PLA/lignin films with varying lignin concentrations. The WCA of pure PLA was 72.9 ± 0.0°, while the WCA of PLA/lignin 1 phr was 74.7 ± 0.6°. The addition of lignin to PLA had no effect on the contact angle value and only improved the hydrophobicity of PLA somewhat. The addition of lignin of the composite films slightly modified the hydrophobic properties of PLA, as the majority of lignin are dispersed in the PLA matrix, not at the surface.

Table 4 WVTR and Contact angle of PLA/lignin composite films.

| Sample | WVTR (g/m$^2$-day) | WCA ($^\circ$) |
|---|---|---|
| PLA | 142.79 | 72.9 ± 0.02 |
| PLA/lignin0.5 | - | 73.6 ± 0.64 |
| PLA/lignin1 | 128.09 | 74.7 ± 0.63 |
| PLA/lignin3 | - | 73.6 ± 0.38 |
| PLA/lignin5 | - | 74.1 ± 0.08 |

## 5.3 Characterization of beeswax coated films

From the results of the above analysis, it was found that the addition of lignin at 1 phr was the most suitable content. This was chosen to be coated with beeswax and analyzed in the next step. There are 2 methods of coating: dipping coating and rod coating.

### 5.3.1 Composite films coated by beeswax by dipping coating

### 5.3.1.1 Morphology

SEM was used to study the surface and cross-sectional area when the films were coated with beeswax. The SEM images of PLA/lignin 1 phr films by beeswax at different concentrations: BW5, BW10, BW15 and BW20 are shown in Figure 46. Figure 46(a, d, g, j) indicate higher surface roughness of the films after coating with higher beeswax concentrations. In addition, the film thickness from images of the cross-sectional is clearly affected with increased thickness as reported in Figure 46(c, f, i, l). The surface is the visible and the irregular plate of wax crystals then distributed in an orderly and densely manner. The higher magnifications are a similar roughness structure that observed flower (5000x magnification) in Figure 46(b, e, h, k) by rapid evaporation of the solvent resulting in a coarse structure of the coating [91].

Surface                                                          Cross-section



(a) BW5 500x magnification    (b) BW5 5000x magnification    (c) BW5 500x magnification

(d) BW10 500x magnification   (e) BW10 5000x magnification   (f) BW10 500x magnification

(g) BW15 500x magnification   (h) BW15 5000x magnification   (i) BW15 500x magnification

(j) BW20 500x magnification   (k) BW20 5000x magnification   (l) BW20 500x magnification
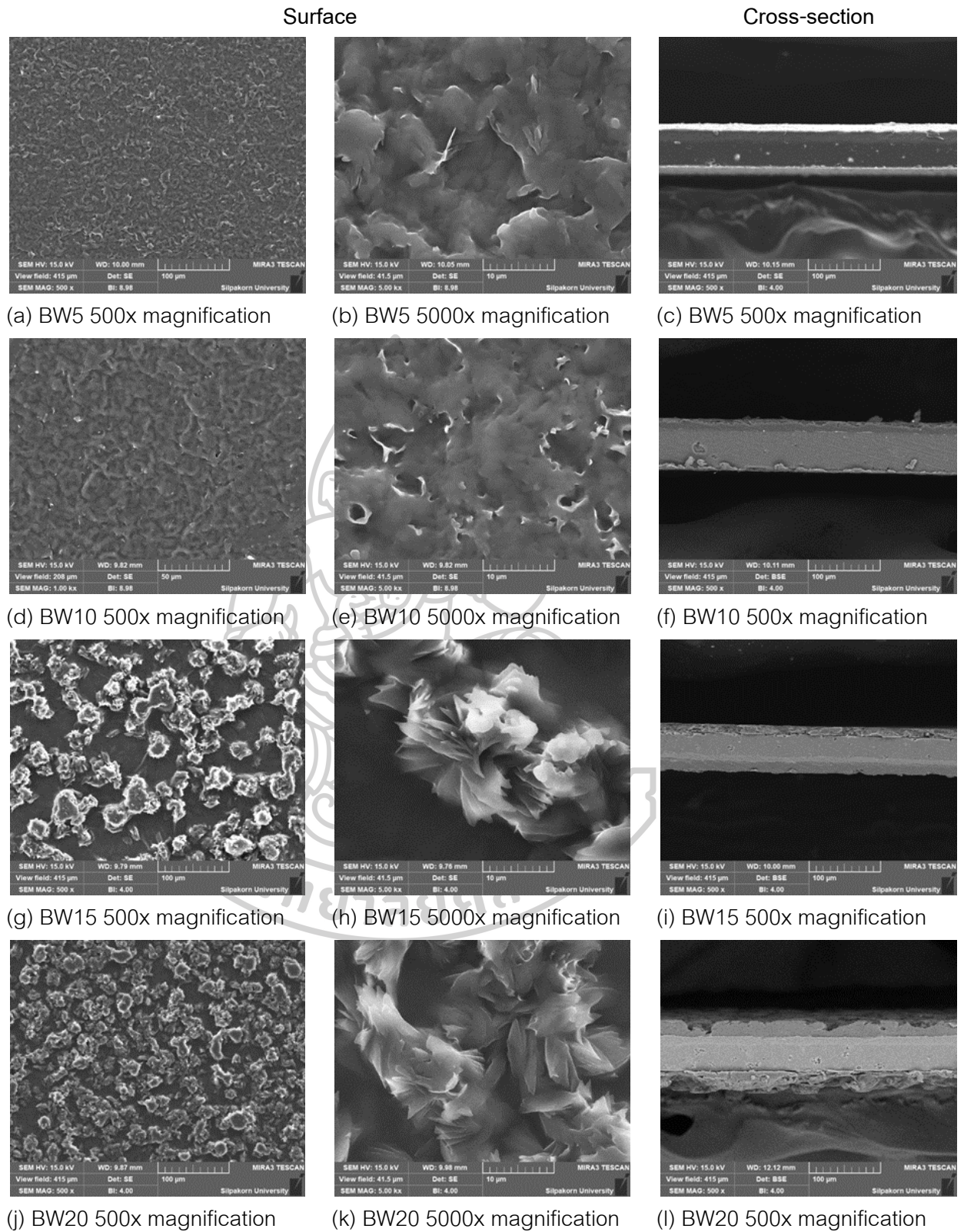
Figure  46 SEM micrographs of PLA/lignin at 1 phr films after coating with different beeswax concentrations.

### 5.3.1.2 FTIR analysis

Beeswax is a complex organic compound system, consisting of hydrocarbons, esters and free fatty acids [92]. FTIR results of beeswax is shown in Figure 47. The absorption bands at 2920 $cm^{-1}$ and 2850 $cm^{-1}$ are hydrocarbons as asymmetric stretching vibrations of $CH_3$ groups and symmetric stretching vibrations of $CH_2$ groups respectively. The peak at 1739 $cm^{-1}$ of the C=O stretching vibrations and at 1172 $cm^{-1}$ of C-H bending vibrations reflect the ester group stretching. The absorption band of fatty acids was observed at 1714 $cm^{-1}$. The fingerprint of beeswax was around 1500-800 $cm^{-1}$ [93]. Additionally, the absorption bands in two peaks are scissor deformation vibrations at 1465 $cm^{-1}$ and rocking vibrations of $CH_2$ groups at 720 $cm^{-1}$. Beeswax is chemically hydrophobic due to its ester group [94].
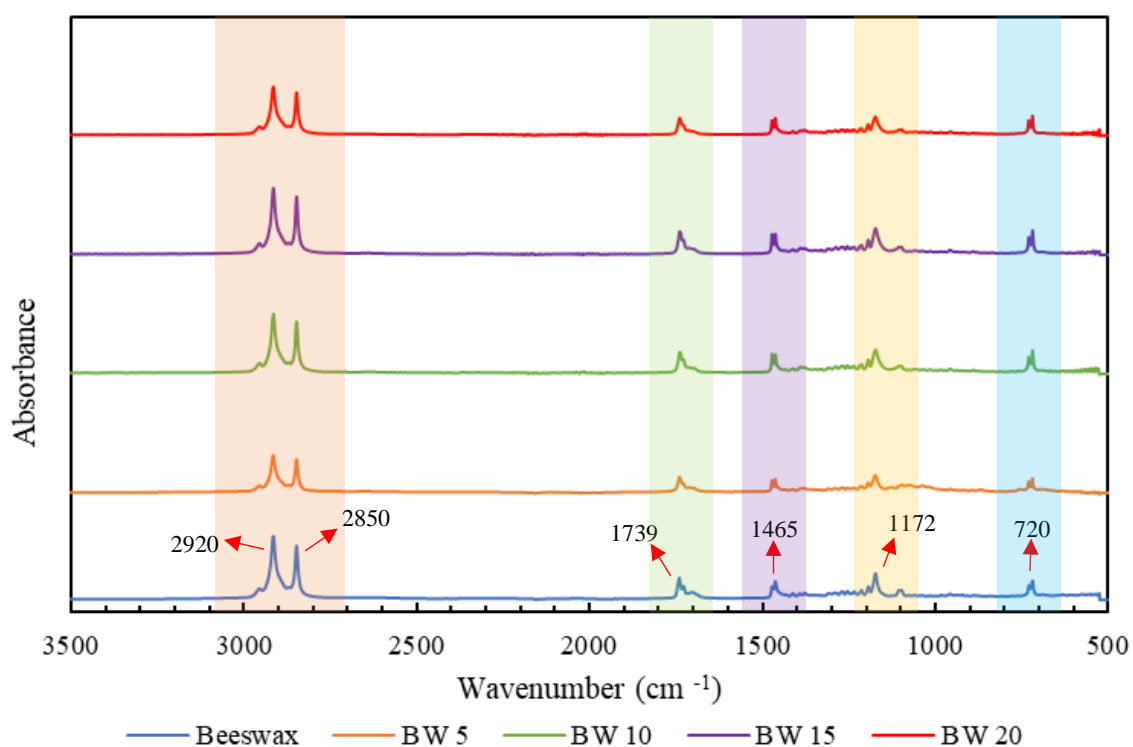


**Figure  47** FTIR spectra of PLA/lignin 1 phr films coated by beeswax by a dipping technique.

### 5.3.1.3 Mechanical properties

The mechanical properties of films are shown in Figure 48-50. The respective the tensile strength, Young's modulus and elongation of the films at different beeswax concentrations was insignificant. The beeswax coating at different concentrations did not affect the mechanical properties of the films. Since it was not blended in polymer matrix also it retains the mechanical properties of the film. The films coated with beeswax at different concentrations caused the film thickness to change. Beeswax was blended with a polymer that reduces its mechanical properties [95]. Therefore, the beeswax was chosen to coat the film surface to maintain the mechanical properties of the film. The higher the concentration is the greater the thickness of the coating layer. The films at BW5, BW10, BW15 and BW20 have a thickness around 0.07, 0.10, 0.11 and 0.12 mm respectively.
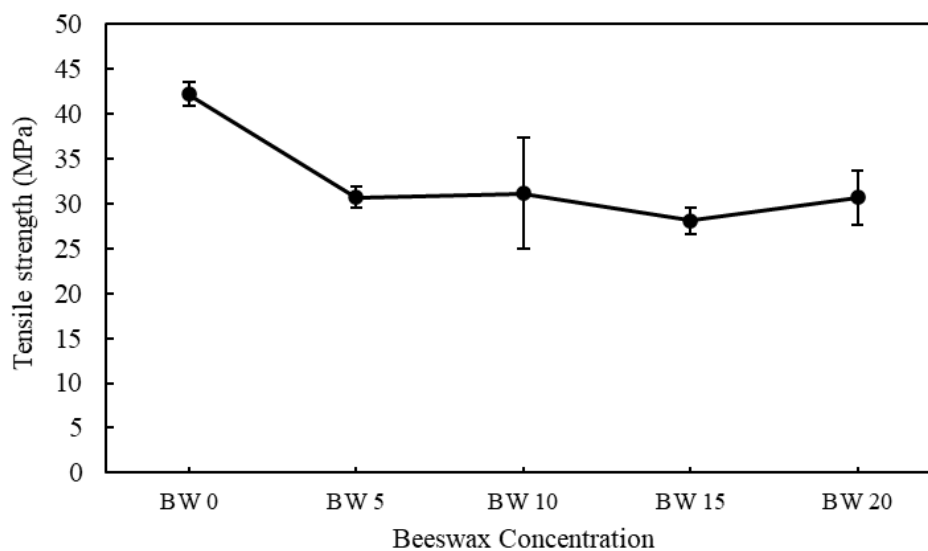


Figure 48 Tensile strength of PLA/lignin 1 phr was dipped at different beeswax concentration.
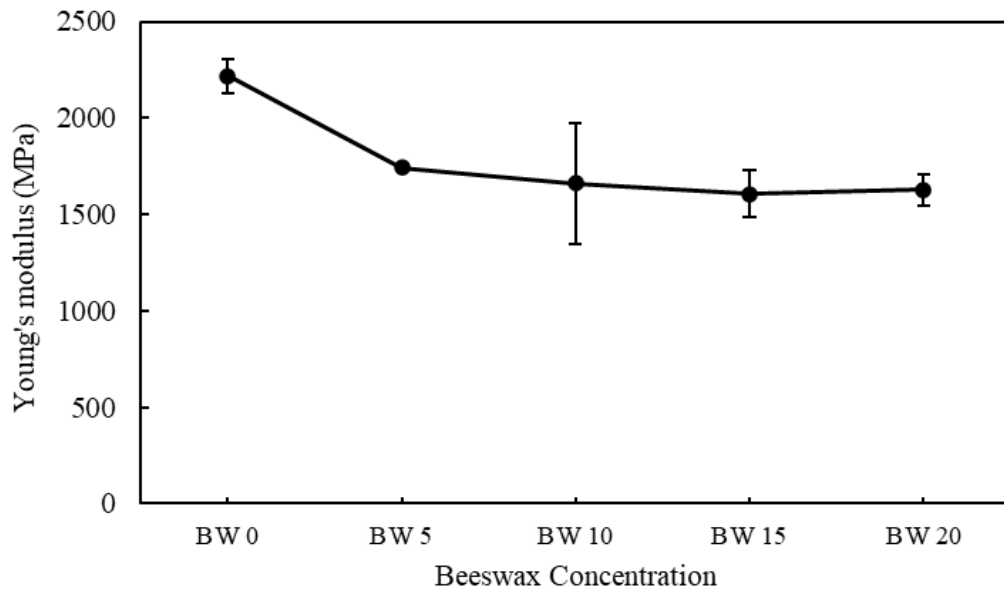
**Figure 49** Young's modulus of PLA/lignin 1 phr was dipped at different beeswax concentration.
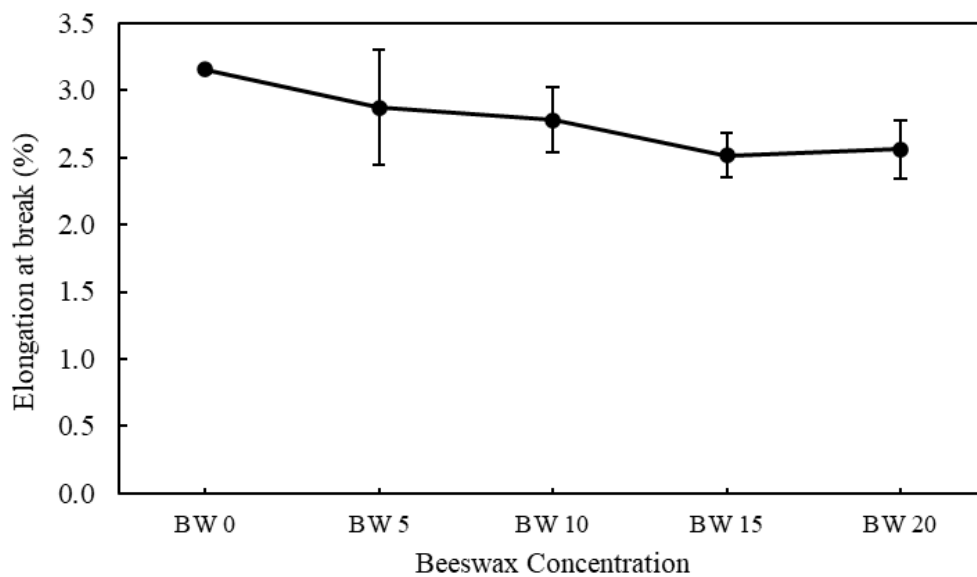


**Figure 50** Elongation at break of PLA/lignin 1 phr was dipped at different beeswax concentration.

### 5.3.1.4 Optical properties

UV light is a high energy that can cause chemical reactions and degrade both polymers and packaged foods. It is important to protect foods sensitive to UV light [10]. As shown in Figure 51, the light barrier property increases with increasing beeswax coating concentration. From the figure observed in the range of 200-300 nm, the minimum percentage of light transmittance is approximately less than 3% transmittance. The UV light range of 200-400 nm is the range that causes lipid oxidation, resulting in rancidity and deterioration [96]. Therefore, the addition of beeswax reduces the transmission of UV light. The increase of beeswax layer thickness reduces the transparency of the film due to the resulting film to be haze so reducing light transmission.
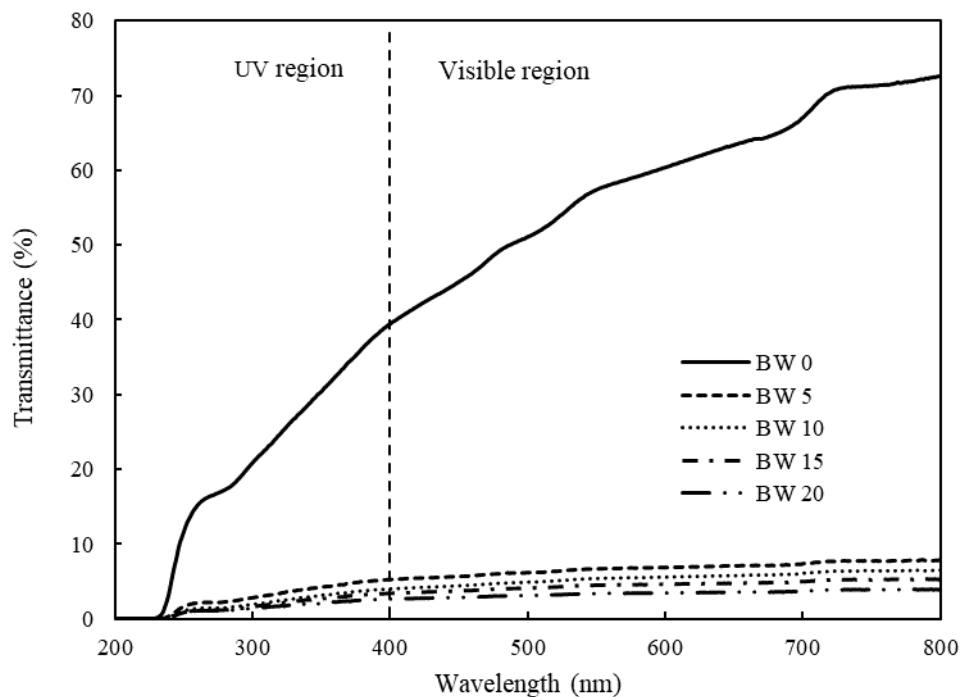


**Figure 51** UV-Vis transmittance spectra for PLA/lignin 1 phr films coated be different beeswax concentration.

### 5.3.1.5 Antioxidant activity

The antioxidant activity was determined by the reduction of DPPH, which free radicals tended to decrease during storage [97]. An antioxidant test was performed by applying the PLA/lignin 1 phr films coated with beeswax concentrations at 0, 5, 10 and 20 %wt. The different beeswax concentrations did not affect the color change, as reported Figure 52. The percent of free radical inhibition scavenging activity assessment is shown in Figure 53. The effect of inhibition was unchanged with increased beeswax concentration, compared to PLA/lignin 1 phr (BW0) at around 80% of inhibition. Therefore, the beeswax does not have the effect of a free radical scavenging [96]. The increase in concentration of beeswax coating does not contribute to free radical scavenging.
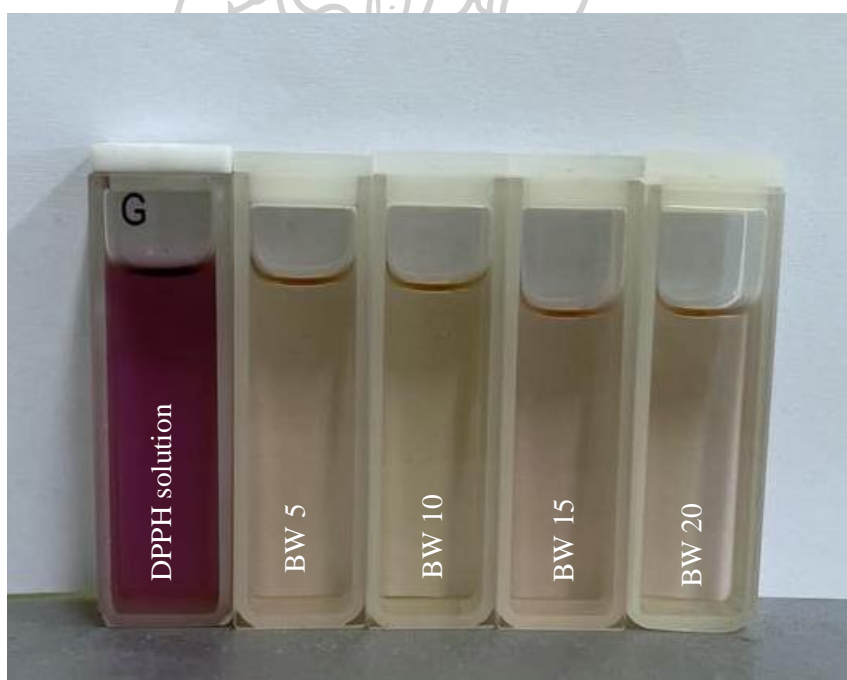


**Figure 52** Color change of DPPH solutions at different beeswax concentrations.
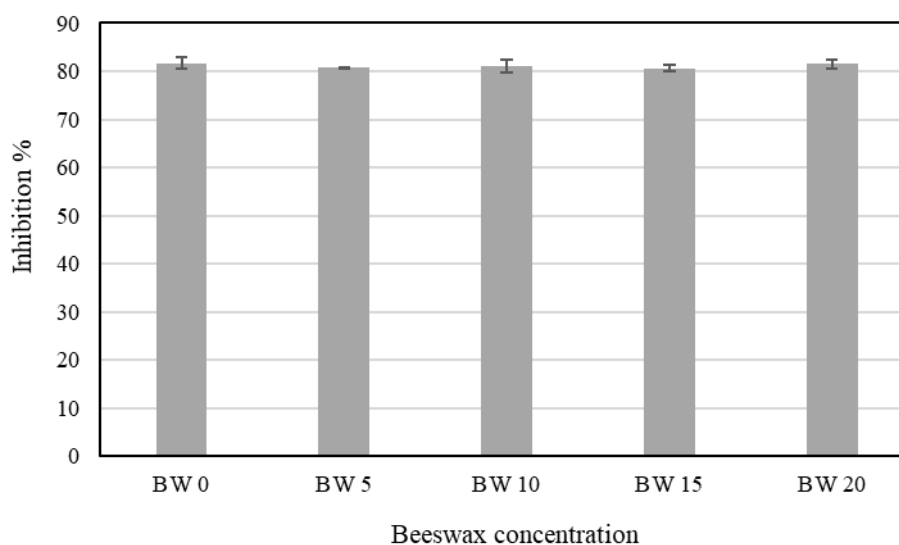
**Figure 53** The percent of free radical inhibition at different beeswax concentration.

**5.3.1.6 Barrier properties**

The results of WVTR and WCA are shown in Table 5.

**5.3.1.6.1 Water vapor transmission rate**

The WVTR results of the films with beeswax-coated and uncoated films were compared. The results showed that beeswax-coated film had a decrease of WVTR from $128.09$ $g/m^2$-day to $40.15$ $g/m^2$-day, representing a percentage reduction of approximately $68\%$. Since, beeswax is more resistant to moisture transfer than other lipid polymers [98]. It is highly resistant to moisture transfer, which reduces water vapor diffusion [99]. In addition, beeswax is highly hydrophobic, so beeswax-coated films are highly resistant to water.

**5.3.1.6.2 Water contact angle**

The water contact angle on the surface of the films coated by different beeswax concentrations: 5, 10, 15 and 20 %wt was measured. The increasing the beeswax concentration resulted an increase the water contact angle. The largest of

increase beeswax concentration at BW 20 was 130.24° which is the best water protection. From the SEM image in Figure 44, the surface of the beeswax-coated film has a rough surface. Because its hydrophobic, it has a very high water resistance and low surface energy [100]. Therefore, the use of beeswax coating can improve its water resistance properties and can be used as a multilayer coating to increase water permeability [101].

Table  5 WVTR and water contact angle of PLA/lignin 1 phr films coated with different beeswax concentrations.

| Sample | WVTR (g/m²-day) | WCA (°) |
|--------|-----------------|---------|
| BW 0   | 128.09          | 74.7 ± 0.63 |
| BW 5   | -               | 106.26 ± 0.11 |
| BW 10  | -               | 117.10 ± 0.21 |
| BW 15  | -               | 123.33 ± 0.16 |
| BW 20  | 40.15           | 130.24 ± 0.48 |

### 5.3.2 Composite films coated by beeswax by rod coating

### 5.3.2.1 Morphology

The beeswax coating by a rod coating machine used a groove size to help controling the film thickness. The beeswax was coated the film used of different groove sizes at 12, 24, 40 and 50 μm, as shown in Figure 54-55. Figure 54 shows that the surface of the beeswax coating layers were nearly the same roughness. In Figure 55, the cross-section of the beeswax coating indicates a coating thickness, which the larger of the groove size effect of the greater the thickness of the beeswax. Therefore, using the groove size of different sizes affects the thickness of the coating.

a) 12 µm

b) 24 µm

c) 40 µm

d) 50 µm
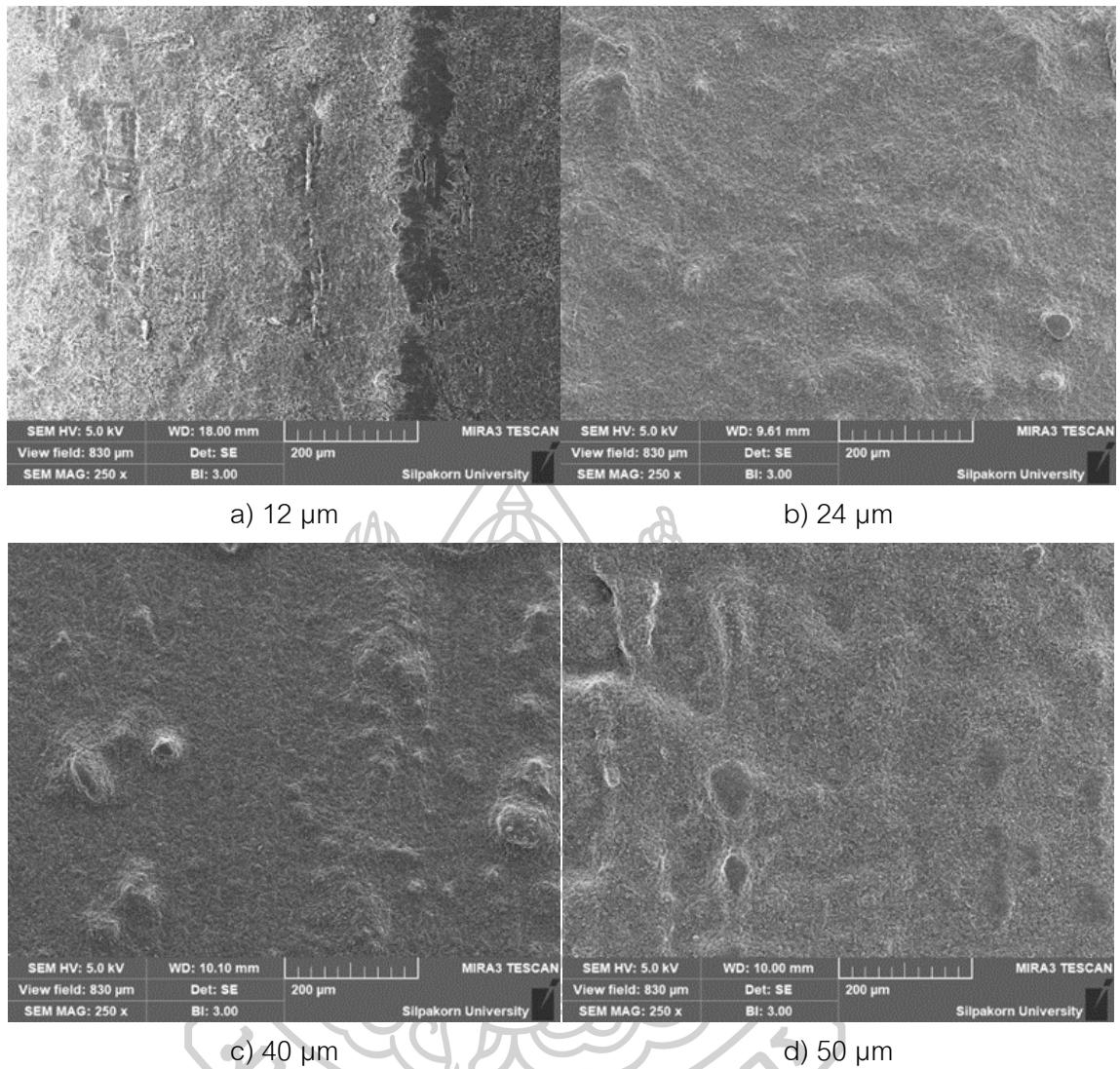
Figure 54 SEM micrographs of surface for beeswax coating by different groove size.

a) 12 µm

b) 24 µm

c) 40 µm

d) 50 µm
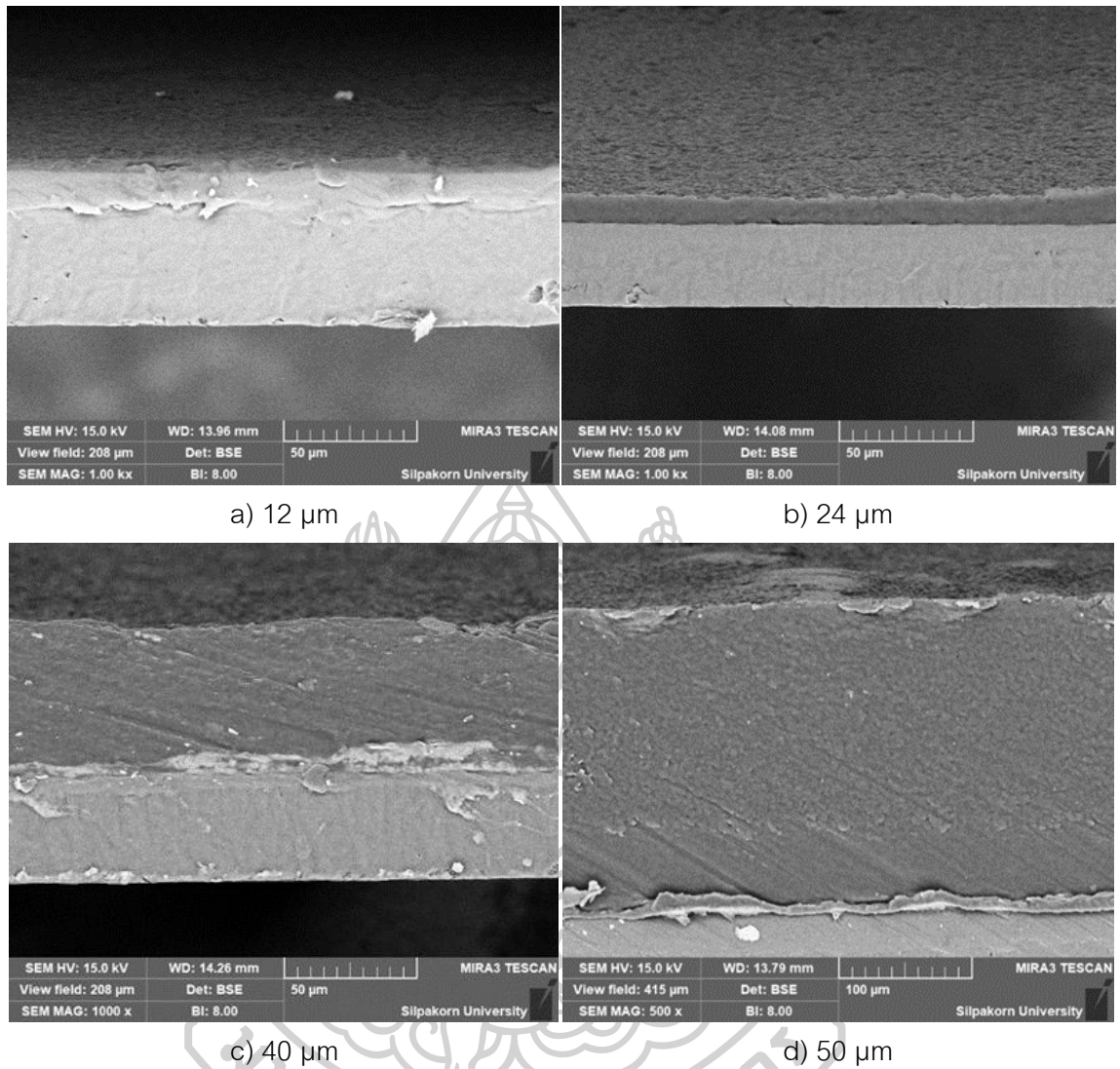
**Figure 55** SEM micrographs of cross-section for beeswax coating by different groove size.

**5.3.2.2 Water contact angle**

The beeswax is already hydrophobic, then coated to the film. The contact angle measurement of the beeswax coated films was measured, as shown in Table 6. The groove size increasing led to an increasing the contact angle values. The coating layer of 50 µm were decreased in the contact angle corresponding to the effect as shown in SEM micrographs. The optimum coating thickness is the 40 µm groove size also increases from 72.9° to 126.5°.

**Table  6** Contact angle of beeswax coating

| Sample | Water contact angle (°) |
|--------|-------------------------|
| PLA    | 72.9 ± 0.02             |
| 12 µm  | 109.7 ± 0.03            |
| 24 µm  | 113.0 ± 0.35            |
| 40 µm  | 126.5 ± 0.11            |
| 50 µm  | 113.7 ± 0.07            |

CHAPTER 6

CONCLUSIONS

Composite films made of PLA and lignin have been developed. Acid precipitation was used to make lignin from black liquor. The PLA/lignin composites of morphology and characteristics were examined. SEM micrographs revealed the presence of lignin as agglomerates distributed on the surface of PLA/lignin. PLA/lignin1 phr revealed a finer PLA/lignin interaction. The 1 phr of lignin may be the best amount to apply to help with interface and mechanical properties. The XRD results show that when lignin was added to PLA the film had less crystalline. When lignin was added at 1phr showed that the film had high thermal stability. Furthermore, lignin has UV protection characteristics, which can aid in the preservation of food quality. The lignin that results is capable of providing a strong UV barrier. The results of an antioxidant test with the addition of lignin showed that at 1 phr it could improve approximately 18% of reduction DPPH. The contact angle data show that the hydrophobic characteristics of lignin were unaffected by its intensification. It was found that the addition of lignin at 1phr was the optimal amount, so PLA/lignin 1 phr films were selected for beeswax coating. To study the effect of beeswax concentrations for the coating that result was increased thickness with the increasing beeswax concentrations. The beeswax coating does not affect mechanical and antioxidant properties of the films. This means it retains good mechanical and antioxidant properties. As for the UV barrier, it gives better UV effect when coated with beeswax. The higher the concentration of beeswax, the thickness and haze of the films with the increase, thus providing good UV protection. As for the effect of water vapor transmission rate and water contact angle, it was found that the optimum concentration of the beeswax coating was at 20% concentration.

As a result, the lignin filler should be used in the optimum amount so that the films can still be used and keep their other features. In this research, the optimum content of lignin was 1 phr. In the beeswax dip coating, the higher beeswax concentration so the better the UV protection properties, water vapor permeability and water contact angle. This may cause the resulting film to become more opaque and thicker.

# REFERENCES

1.    Majhi, S., A. Tyagi, and A. Mishra, *Bio-polymeric packaging material for packaging of raw food.* 2019.

2.    Yadav, A., et al., *Biopolymers as packaging material in food and allied industry.* 2018.

3.    Pereira de Abreu, D., J.M. Cruz, and P. Paseiro Losada, *Active and intelligent packaging for the food industry.* Food Reviews International, 2012. **28**(2): p. 146-187.

4.    Miao, L., et al., *Characterization of polylactic acids-polyhydroxybutyrate based packaging film with fennel oil, and its application on oysters.* Food Packaging and Shelf Life, 2019. **22**: p. 100388.

5.    Mohamad, N., et al., *Development of active agents filled polylactic acid films for food packaging application.* International Journal of Biological Macromolecules, 2020. **163**: p. 1451-1457.

6.    Domenek, S., et al., *Potential of lignins as antioxidant additive in active biodegradable packaging materials.* Journal of Polymers and the Environment, 2013. **21**(3): p. 692-701.

7.    Rukmanikrishnan, B., et al., *Binary and ternary sustainable composites of gellan gum, hydroxyethyl cellulose and lignin for food packaging applications: Biocompatibility, antioxidant activity, UV and water barrier properties.* International journal of biological macromolecules, 2020. **153**: p. 55-62.

8.    Fratini, F., et al., *Beeswax: A minireview of its antimicrobial activity and its application in medicine.* Asian Pacific Journal of Tropical Medicine, 2016. **9**(9): p. 839-843.

9.    Zhang, Y., et al., *Functional food packaging for reducing residual liquid food: Thermo-resistant edible super-hydrophobic coating from coffee and beeswax.* Journal of colloid and interface science, 2019. **533**: p. 742-749.

10.   Mohd Aris, Z.F., et al., *Barrier properties and abrasion resistance of biopolymer-*

*based coatings on biodegradable poly (lactic acid) films.* Polymer Engineering & Science, 2019. **59**(9): p. 1874-1881.

11.  Byun, Y. and Y.T. Kim, *Bioplastics for food packaging: chemistry and physics*, in *Innovations in food packaging*. 2014, Elsevier. p. 353-368.

12.  Tham, C., et al., *Surface engineered poly (lactic acid)(PLA) microspheres by chemical treatment for drug delivery system*. Vol. 594. 2014: Trans Tech Publ.

13.  Hagen, R., *Polylactic Acid.* 2012.

14.  de Moura, I.G., et al., *Bioplastics from agro-wastes for food packaging applications*, in *Food Packaging*. 2017, Elsevier. p. 223-263.

15.  Xu, C. and F. Ferdosian, *Conversion of lignin into bio-based chemicals and materials*. 2017: Springer.

16.  Huber, G.W., S. Iborra, and A. Corma, *Synthesis of transportation fuels from biomass: chemistry, catalysts, and engineering.* Chemical reviews, 2006. **106**(9): p. 4044-4098.

17.  Hatakeyama, H. and T. Hatakeyama, *Lignin structure, properties, and applications*, in *Biopolymers*. 2009, Springer. p. 1-63.

18.  Khan, T.A., J.-H. Lee, and H.-J. Kim, *Lignin-Based Adhesives and Coatings*, in *Lignocellulose for Future Bioeconomy*. 2019. p. 153-206.

19.  Szulc, J., et al., *Beeswax-Modified Textiles: Method of Preparation and Assessment of Antimicrobial Properties*. Polymers, 2020. **12**(2): p. 344.

20.  WAX, B.P., *Beeswax: Production, Properties Composition and Control.*

21.  Bonvehi, J.S. and F.O. Bermejo, *Detection of adulterated commercial Spanish beeswax.* Food chemistry, 2012. **132**(1): p. 642-648.

22.  Bogdanov, S., *Beeswax: quality issues today.* Bee World, 2004. **85**(3): p. 46-50.

23.  Roy, S. and N.R. Singha, *Polymeric nanocomposite membranes for next generation pervaporation process: Strategies, challenges and future prospects.* Membranes, 2017. **7**(3): p. 53.

24.  Pinto, A.M., V.S. Oliveira, and D.S.C. Falcão, *Direct alcohol fuel cells for portable applications: fundamentals, engineering and advances*. 2018: Academic Press.

25.    Homma, Y., *III–V Growth, In Situ Observation by Scanning Electron Microscopy of.* 2001.

26.    Garbacz, H. and A. Królikowski, *Corrosion resistance of nanocrystalline titanium*, in *Nanocrystalline Titanium*. 2019, Elsevier. p. 145-173.

27.    Kannan, M., *Scanning Electron Microscopy: Principle, Components and Applications.*

28.    Wang, Q.J. and Y.-W. Chung, *Encyclopedia of tribology*. 2013: Springer.

29.    Cruz, I.F., et al., *Chapter 3 - Multifunctional Ferrite Nanoparticles: From Current Trends Toward the Future*, in *Magnetic Nanostructured Materials*, A.A. El-Gendy, J.M. Barandiarán, and R.L. Hadimani, Editors. 2018, Elsevier. p. 59-116.

30.    Sabarinathan, C., S. Muthu, and M.N. Ali. *Experimental Study On Tensile Behavior Of Multi Wall Carbon Nanotube Reinforced Epoxy Composites*. 2012.

31.    Gill, P., T.T. Moghadam, and B. Ranjbar, *Differential scanning calorimetry techniques: applications in biology and nanoscience.* Journal of biomolecular techniques: JBT, 2010. **21**(4): p. 167.

32.    Dollimore, D., *Thermal Analysis*, in *Encyclopedia of Physical Science and Technology (Third Edition)*, R.A. Meyers, Editor. 2003, Academic Press: New York. p. 591-612.

33.    Mohamed, M.A., et al., *Chapter 1 - Fourier Transform Infrared (FTIR) Spectroscopy*, in *Membrane Characterization*, N. Hilal, et al., Editors. 2017, Elsevier. p. 3-29.

34.    Di Gianfrancesco, A., *8 - Technologies for chemical analyses, microstructural and inspection investigations*, in *Materials for Ultra-Supercritical and Advanced Ultra-Supercritical Power Plants*, A. Di Gianfrancesco, Editor. 2017, Woodhead Publishing. p. 197-245.

35.    Houck, M.M. and J.A. Siegel, *Chapter 5 - Light and Matter*, in *Fundamentals of Forensic Science (Third Edition)*, M.M. Houck and J.A. Siegel, Editors. 2015, Academic Press: San Diego. p. 93-119.

36.    Gällstedt, M. and M.S. Hedenqvist, *Packaging‑related properties of alkyd‑coated,*

*wax -coated, and buffered chitosan and whey protein films.* Journal of applied polymer science, 2004. **91**(1): p. 60-67.

37.     Dwivedi, C., et al., *Chapter 9 - Electrospun Nanofibrous Scaffold as a Potential Carrier of Antimicrobial Therapeutics for Diabetic Wound Healing and Tissue Regeneration*, in *Nano- and Microscale Drug Delivery Systems*, A.M. Grumezescu, Editor. 2017, Elsevier. p. 147-164.

38.     Kulkarni, V.S. and C. Shaw, *Chapter 2 - Surfactants, Lipids, and Surface Chemistry*, in *Essential Chemistry for Formulators of Semisolid and Liquid Dosages*, V.S. Kulkarni and C. Shaw, Editors. 2016, Academic Press: Boston. p. 5-19.

39.     Shahidi, F. and Y. Zhong, *Measurement of antioxidant activity.* Journal of functional foods, 2015. **18**: p. 757-781.

40.     Nenadis, N. and M. Tsimidou, *Assessing the activity of natural food antioxidants*, in *Oxidation in foods and beverages and antioxidant applications*. 2010, Elsevier. p. 332-367.

41.     Bondet, V., W. Brand-Williams, and C. Berset, *Kinetics and mechanisms of antioxidant activity using the DPPH. free radical method.* LWT-Food Science and Technology, 1997. **30**(6): p. 609-615.

42.     Kedare, S.B. and R. Singh, *Genesis and development of DPPH method of antioxidant assay.* Journal of food science and technology, 2011. **48**(4): p. 412-422.

43.     Mishra, K., H. Ojha, and N.K. Chaudhury, *Estimation of antiradical properties of antioxidants using DPPH assay: A critical review and results.* Food chemistry, 2012. **130**(4): p. 1036-1043.

44.     Duval, A. and M. Lawoko, *A review on lignin-based polymeric, micro-and nano-structured materials.* Reactive and Functional Polymers, 2014. **85**: p. 78-96.

45.     Bahl, K., T. Miyoshi, and S.C. Jana, *Hybrid fillers of lignin and carbon black for lowering of viscoelastic loss in rubber compounds.* Polymer, 2014. **55**(16): p. 3825-3835.

46. Liu, Z., et al. *Extraction of lignin from pulping black liquor by organic acid*. in *Materials Science Forum*. 2009. Trans Tech Publ.

47. Kamble, S. and Y. Bhattacharyulu, *Selective separation of biomass from black liquor waste by inorganic and organic acids.* Int J Adv Res, 2015. **3**(1): p. 684-692.

48. Lim, L.-T., R. Auras, and M. Rubino, *Processing technologies for poly (lactic acid).* Progress in polymer science, 2008. **33**(8): p. 820-852.

49. Erdohan, Z.Ö., B. Çam, and K.N. Turhan, *Characterization of antimicrobial polylactic acid based films.* Journal of Food Engineering, 2013. **119**(2): p. 308-315.

50. Byun, Y., et al., *The effect of solvent mixture on the properties of solvent cast polylactic acid (PLA) film.* Journal of applied polymer science, 2012. **124**(5): p. 3577-3582.

51. Kai, D., et al., *Towards lignin-based functional materials in a sustainable world.* Green Chemistry, 2016. **18**(5): p. 1175-1200.

52. Li, X., et al., *Poly (lactic acid)/lignin blends prepared with the Pickering emulsion template method.* European Polymer Journal, 2019. **110**: p. 378-384.

53. Yang, W., et al., *Poly (lactic acid)/lignin films with enhanced toughness and anti-oxidation performance for active food packaging.* International journal of biological macromolecules, 2020. **144**: p. 102-110.

54. Shankar, S. and J.-W. Rhim, *Preparation and characterization of agar/lignin/silver nanoparticles composite films with ultraviolet light barrier and antibacterial properties.* Food Hydrocolloids, 2017. **71**: p. 76-84.

55. Qian, Y., X. Qiu, and S. Zhu, *Sunscreen performance of lignin from different technical resources and their general synergistic effect with synthetic sunscreens.* ACS Sustainable Chemistry & Engineering, 2016. **4**(7): p. 4029-4035.

56. Dizhbite, T., et al., *Characterization of the radical scavenging activity of lignins—natural antioxidants.* Bioresource technology, 2004. **95**(3): p. 309-317.

57. Bang, G. and S.W. Kim, *Biodegradable poly (lactic acid)-based hybrid coating materials for food packaging films with gas barrier properties.* Journal of Industrial

and Engineering Chemistry, 2012. **18**(3): p. 1063-1068.

58. Navarro-Tarazaga, M.L., R. Sothornvit, and M.a.B. Pérez-Gago, *Effect of plasticizer type and amount on hydroxypropyl methylcellulose━ beeswax edible film properties and postharvest quality of coated plums (cv. Angeleno).* Journal of Agricultural and Food Chemistry, 2008. **56**(20): p. 9502-9509.

59. Reis, M.O., et al., *Biodegradable trays of thermoplastic starch/poly (lactic acid) coated with beeswax.* Industrial Crops and Products, 2018. **112**: p. 481-487.

60. Park, Y.D., et al., *Post-deposition dipping method for improving the electronic properties of a narrow bandgap conjugated polymer.* Journal of Materials Chemistry, 2012. **22**(23): p. 11462-11465.

61. Tan, M., et al., *Solvent effect on the formation of self-assembled monolayer on DLC surface between n-hexane and Vertrel XF.* Applied surface science, 2008. **254**(20): p. 6332-6336.

62. Latthe, S.S., et al., *Self–cleaning superhydrophobic coatings: Potential industrial applications.* Progress in Organic Coatings, 2019. **128**: p. 52-58.

63. Namane, M., et al., *Characteristics of lignin precipitated with organic acids as a source for valorisation of carbon products.* Cellulose Chemistry and Technology, 2016. **50**(3-4): p. 355-360.

64. Hamzah, M., S. Bowra, and P. Cox, *Purity and structural composition of lignin isolated from Miscanthus x giganteus by sub-critical water extraction with associated modifiers.* J. Agric. Food Eng, 2020. **1**: p. 1-12.

65. Triwulandari, E., et al., *Effect of lignin on mechanical, biodegradability, morphology, and thermal properties of polypropylene/polylactic acid/lignin biocomposite.* Plastics, Rubber and Composites, 2019. **48**(2): p. 82-92.

66. Bužarovska, A., et al., *Poly (l-lactic acid)/alkali lignin composites: properties, biocompatibility, cytotoxicity and antimicrobial behavior.* Journal of Materials Science, 2021. **56**(24): p. 13785-13800.

67. Furukawa, T., et al., *Comparison of miscibility and structure of poly (3-hydroxybutyrate-co-3-hydroxyhexanoate)/poly (l-lactic acid) blends with those of*

*poly (3-hydroxybutyrate)/poly (l-lactic acid) blends studied by wide angle X-ray diffraction, differential scanning calorimetry, and FTIR microspectroscopy.* Polymer, 2007. **48**(6): p. 1749-1755.

68. de Baynast, H., et al., *Effects of Kraft lignin and corn cob agro-residue on the properties of injected-moulded biocomposites.* Industrial Crops and Products, 2022. **177**: p. 114421.

69. Syazwan, M. and T. Sasaki, *Rapid crystallization and mesophase formation of poly (L-lactic acid) during precipitation from a solution.* e-Polymers, 2018. **18**(4): p. 331-337.

70. Zhang, G., et al., *Miscibility and phase structure of binary blends of polylactide and poly (vinylpyrrolidone).* Journal of Applied Polymer Science, 2003. **88**(4): p. 973-979.

71. Ye, H., Y. Zhang, and Z. Yu, *Effect of desulfonation of lignosulfonate on the properties of poly (lactic acid)/lignin composites.* BioResources, 2017. **12**(3): p. 4810-4829.

72. Wang, X., et al., *Thermal, mechanical, and degradation properties of nanocomposites prepared using lignin-cellulose nanofibers and poly (lactic acid).* BioResources, 2014. **9**(2): p. 3211-3224.

73. Das, K., et al., *Crystalline morphology of PLA/clay nanocomposite films and its correlation with other properties.* Journal of applied polymer science, 2010. **118**(1): p. 143-151.

74. Lui, F.H.Y., et al., *The effects of chemical components and particle size on the mechanical properties of binderless boards made from oak (Quercus spp.) logs degraded by shiitake fungi (Lentinula edodes).* Journal of Wood Science, 2018. **64**(3): p. 246-255.

75. Yang, W., et al., *Synergic effect of cellulose and lignin nanostructures in PLA based systems for food antibacterial packaging.* European Polymer Journal, 2016. **79**: p. 1-12.

76. Ghozali, M. and E.N. Rohmah. *Synthesis of PP-g-MA as compatibilizer for PP/PLA*

*biocomposites: Thermal, mechanical and biodegradability properties.* in *AIP Conference Proceedings.* 2017. AIP Publishing LLC.

77. Sarfraz, A., et al., *Electrode Materials for Fuel Cells,* in *Reference Module in Materials Science and Materials Engineering.* 2020, Elsevier.

78. Gordobil, O., et al., *Physicochemical properties of PLA lignin blends.* Polymer Degradation and Stability, 2014. **108**: p. 330-338.

79. Bertini, F., et al., *Effect of ligno-derivatives on thermal properties and degradation behavior of poly(3-hydroxybutyrate)-based biocomposites.* Polymer Degradation and Stability, 2012. **97**(10): p. 1979-1987.

80. Morandim-Giannetti, A.A., et al., *Lignin as additive in polypropylene/coir composites: Thermal, mechanical and morphological properties.* Carbohydrate Polymers, 2012. **87**(4): p. 2563-2568.

81. Yang, W., et al., *Effect of lignin nanoparticles and masterbatch procedures on the final properties of glycidyl methacrylate-g-poly (lactic acid) films before and after accelerated UV weathering.* Industrial Crops and Products, 2015. **77**: p. 833-844.

82. Guo, J., et al., *The influence of compatibility on the structure and properties of PLA/lignin biocomposites by chemical modification.* Polymers, 2020. **12**(1): p. 56.

83. Abdelwahab, M.A., et al., *Thermo-mechanical characterization of bioblends from polylactide and poly (butylene adipate-co-terephthalate) and lignin.* Macromolecular Materials and Engineering, 2015. **300**(3): p. 299-311.

84. Li, X., et al., *Poly(lactic acid)/lignin blends prepared with the Pickering emulsion template method.* European Polymer Journal, 2019. **110**: p. 378-384.

85. Simmons, T.J., et al., *Preparation of synthetic wood composites using ionic liquids.* Wood science and technology, 2011. **45**(4): p. 719-733.

86. Sadeghifar, H. and A. Ragauskas, *Lignin as a UV light blocker—a review.* Polymers, 2020. **12**(5): p. 1134.

87. Huang, D., B. Ou, and R.L. Prior, *The chemistry behind antioxidant capacity assays.* Journal of agricultural and food chemistry, 2005. **53**(6): p. 1841-1856.

88. de Menezes Nogueira, I., et al., *Organic solvent fractionation of acetosolv palm oil*

*lignin: The role of its structure on the antioxidant activity.* International journal of biological macromolecules, 2019. **122**: p. 1163-1172.

89.  Bork, M., *An overview of the influences on the properties of lignin-PLA composites for the purpose of food packaging.* 2020.

90.  Shankar, S., J.-W. Rhim, and K. Won, *Preparation of poly (lactide)/lignin/silver nanoparticles composite films with UV light barrier and antibacterial properties.* International journal of biological macromolecules, 2018. **107**: p. 1724-1731.

91.  Shen, T., et al., *Preparation of edible non-wettable coating with soybean wax for repelling liquid foods with little residue.* Materials, 2020. **13**(15): p. 3308.

92.  Sveč njak, L., et al., *An approach for routine analytical detection of beeswax adulteration using FTIR-ATR spectroscopy.* Journal of apicultural science, 2015. **59**(2): p. 37-49.

93.  Tanner, N. and B. Lichtenberg‑Kraag, *Identification and Quantification of Single and Multi‑Adulteration of Beeswax by FTIR‑ATR Spectroscopy.* European Journal of Lipid Science and Technology, 2019. **121**(12): p. 1900245.

94.  Wang, D., et al., *Durable mixed edible wax coating with stretching superhydrophobicity.* Journal of Materials Chemistry A, 2021. **9**(3): p. 1495-1499.

95.  Gontard, N., et al., *Edible composite films of wheat gluten and lipids: water vapour permeability and other physical properties.* International journal of food science & technology, 1994. **29**(1): p. 39-50.

96.  Zhang, Y., B.K. Simpson, and M.-J. Dumont, *Effect of beeswax and carnauba wax addition on properties of gelatin films: A comparative study.* Food bioscience, 2018. **26**: p. 88-95.

97.  Sousa, F.F., et al., *Conservation of 'palmer'mango with an edible coating of hydroxypropyl methylcellulose and beeswax.* Food Chemistry, 2021. **346**: p. 128925.

98.  Velickova, E., et al., *Characterization of multilayered and composite edible films from chitosan and beeswax.* Food Science and Technology International, 2015. **21**(2): p. 83-93.

99.     Oliveira, V., et al., *Use of biopolymeric coating hydrophobized with beeswax in post-harvest conservation of guavas.* Food chemistry, 2018. **259**: p. 55-64.

100.    Han, J.H., *Edible films and coatings: a review.* Innovations in food packaging, 2014: p. 213-255.

101.    Liu, K., et al., *Preparation of the CNC/Ag/beeswax composites for enhancing antibacterial and water resistance properties of paper.* Carbohydrate polymers, 2016. **142**: p. 183-188.

# VITA

| | |
|---|---|
| NAME | Arphaphorn Arjhan |
| DATE OF BIRTH | 12 Jan 1997 |
| PLACE OF BIRTH | Ratchaburi |
| HOME ADDRESS | 122/1 M.3 Pakrat Banpong Ratchaburi 70110 |